The 3-d 3-state Potts model with a non-zero density of static color charges

Masterarbeit

der Philosophisch-naturwissenschaftlichen Fakultät
der Universität Bern
vorgelegt von

Philippe Widmer

2011

Betreut durch

Prof. Dr. U.-J. Wiese

Albert Einstein Center for Fundamental Physics
Institut für Theoretische Physik, Universität Bern

Abstract

We calculate the phase diagram of the 3-dimensional 3-state Potts model with an additional non-zero density of infinitely heavy color charges as a model for QCD with heavy quarks. This model has a sign problem which can be solved by a meron-cluster algorithm. This algorithm is theoretically ergodic but practically it is nearly impossible to reach certain configurations, as will be explained, making it very hard to accurately calculate some physical quantities. To circumvent this problem we use a variant of a flux model which is equivalent to the Potts model. The physical observables are easily calculable there using a worm algorithm.

We found that the first order phase transition from the original Potts model without color charges is weakened by increasing the number of charges. At some point it probably turns into a second order transition before finally disappearing completely. However, because of a lack of time, locating the exact point where the transition becomes second order was not possible and we were unable to identify the details of where and how the transition vanishes.

Contents

1. Introduction

The theory of the strong force, Quantum Chromodynamics (QCD), seems to have (at least) two phases: the low energy confined phase where the quarks are bound into colorless states and the high energy deconfined phase where quarks can exist as quasi-free particles. This is a highly non-perturbative feature of QCD which can be investigated from first principles only by using the lattice regularization which will be explained briefly in chapter 2. In fact it hasn't even been rigorously proven yet for full QCD. In some simplified cases, however, it is possible to analytically study confinement. For example in Yang-Mills theory with static quarks and infinite coupling constant confinement is already established, i.e. in this system the quarks (and gluons) are indeed confined (as will be shown in this thesis). For all other values of the coupling constant and for most more complicated systems, the problem can only be solved numerically using Monte Carlo simulations. However, this is presently still a very difficult task. Even though pure Yang-Mills theory doesn't pose any unsurmountable problems, adding quarks or, more generally, fermions often introduces a so-called complex action problem. The standard way to simulate a system with many degrees of freedom is to use Monte Carlo simulations which generate configurations based on a probability distribution, i.e. they generate the more probable ones more often. Normally one uses the Boltzmann factor $\exp(-S)$ as a probability distribution. If S is not real and positive, one encounters the complex action problem. Interpreting the action as a probability distribution then obviously doesn't work. This problem can be quite hard to solve depending on the actual model. It still remains unsolved for QCD even though some progress has been made lately ([6] contains an overview of the techniques used and the results of some recent work).

An easier way is to use simplified models which share some key features with the full model. An example of this is the so-called 3-dimensional 3-state Potts model which we will be using here. Calculating the phase transition numerically in this model using a cluster algorithm is a task already performed by other people [1, 4].

The standard Potts model does not include an equivalent to quarks. It represents pure Yang-Mills theory, a theory consisting only of gluons. Adding static charges as a model for infinitely heavy quarks has already been done a number of times [1, 4, 10]. These works introduce a chemical potential coupling to the quark number Q. In order for the quarks to be truly static, their mass M has to be set to infinity. To avoid getting only trivial results, the chemical potential has to go to infinity as well such that $M - \mu$ remains finite. This then means that using these simplifications, only a small part of the whole phase diagram can be studied, namely only the case of systems with many infinitely heavy quarks. It was found that there is a line of first order transition starting at the transition point of the original Potts model. It ends at a critical end point to finally turn into a crossover [1]. Using only this approach still leaves a complex action problem, i.e. it is not possible to easily simulate this model using standard Monte Carlo algorithms. In recent work [10] an improved algorithm for an equivalent model was used to circumvent this problem. This study still found a region with a first order phase transition and a crossover everywhere else.

In this thesis we will use a similar approach for a slightly different model. We want to add a fixed number of static color charges to the Potts model, i.e. without introducing a chemical potential. We obtain a representation of these infinitely heavy quarks by using Polyakov loops which is the standard way to achieve this in Yang-Mills theory. This introduces a complex action problem. Solving it is possible using a so-called meron-cluster algorithm, the construction of which will be explained in chapter 3. This completely solves the complex

action problem but still leaves a dynamical problem: The algorithm is practically non-ergodic because the system may get stuck in the so-called two-meron sector which, as will be shown in this thesis, prevents the calculation of useful results or at least greatly decreases the amount of statistics generated.

At this point we can then use a similar solution to what has been done in [10]: We switch to a different but equivalent model where there is no complex action problem at all. This new model is called the flux model as its fundamental degrees of freedom are static charges and (charge) fluxes in between. It can be efficiently simulated using so-called worm algorithms introduced (for different problems) by N. Prokof'ev and B. Svistunov [13, 14]. This also avoids the problem with the two-meron sector of the Potts model completely. All this will be explained in chapter 4.

As the flux model solves these problems we are then in a position to start calculating the phase diagram of the Potts model with a fixed number of static color charges. How one can then proceed to calculate the diagram is explained in the first part of chapter 5. The second part and the conclusion of this work consist of a discussion of our results (and some problems that still remain).

2. Lattice Quantum Chromodynamics with static quarks

We want to investigate the confinement-deconfinement phase transition in a theory based on Quantum Chromodynamics (QCD) without dynamical quarks. This leaves us with the gluon gauge fields and infinitely heavy color charges representing static quarks. We start by introducing the general concepts of lattice QCD.

2.1. Pure gauge lattice Yang-Mills theory

Standard pure gauge Yang-Mills theory in the path integral formulation with Euclidean time can be defined using its partition function

$$Z = \int \mathcal{D}G \, \exp(-S[G]), \tag{2.1}$$

where the action is

$$S[G] = -\int d^4x \, \frac{1}{4g_s^2} \mathrm{tr} G_{\mu\nu} G_{\mu\nu} \tag{2.2}$$

and

$$G_{\mu\nu}(x) = \partial_\mu G_\nu(x) - \partial_\nu G_\mu(x) + [G_\mu(x), G_\nu(x)], \tag{2.3}$$

$$G_\mu(x) = i g_s G_\mu^a(x) T^a, \quad a = 1, ..., 8. \tag{2.4}$$

Here T^a are the generators of the gauge group $SU(N)$ and $G_\mu^a(x)$ are the gluon fields transforming in the adjoint representation of $SU(N)$. In order to be well defined, the meaning of the integral measure $\mathcal{D}G$ needs to be clarified. In general this is a product of infinitely many integrals (one for each point in space-time since there is an independent field variable $G(x)$ for each x) over the group space of $SU(N)$. The only possible way to define this currently (apart from perturbative expansions) is to regularize it by introducing a space-time lattice. The continuum theory is then defined by taking the limit of vanishing lattice spacing.

The lattice is introduced by replacing for each dimension of space-time the continuous real numbers by integers and by introducing a lattice spacing a between adjacent lattice points. As a representation of the gauge fields one then adds so-called link variables $U_{\mu,x} \in SU(N)$ on the line connecting the point x to $x + a\hat{\mu}$ in the positive μ-direction (where $\hat{\mu}$ is a unit-vector in this direction) as shown in figure 1. These link variables take values in the group $SU(N)$ and one can write

$$U_{\mu,x} = \exp\left(a G_\mu \left(x + \frac{a\hat{\mu}}{2} \right) \right), \tag{2.5}$$

which ensures that for vanishing lattice spacing the link variables become the gauge fields at the point x because

$$U_{\mu,x} = \mathbf{1} + a G_\mu \left(x + \frac{a\hat{\mu}}{2} \right) + O(a^2). \tag{2.6}$$

Under gauge transformations these fields transform as

$$U'_{\mu,x} = \Omega_x U_{\mu,x} \Omega^\dagger_{x+a\hat{\mu}}, \quad \Omega_x \in SU(N), \tag{2.7}$$

which yields after a short calculation using $a \to 0$ in continuum notation

$$U'_{\mu,x} = \mathbf{1} + a\Omega(x)\left[G_\mu(x) + \partial_\mu\right]\Omega(x)^\dagger + O(a^2). \tag{2.8}$$

Together with formula (2.6) this shows that in the continuum limit the gauge field transforms correctly, i.e.

$$G'_\mu(x) = \Omega(x)(G_\mu(x) + \partial_\mu)\Omega(x)^\dagger, \quad \Omega(x) \in SU(N). \tag{2.9}$$

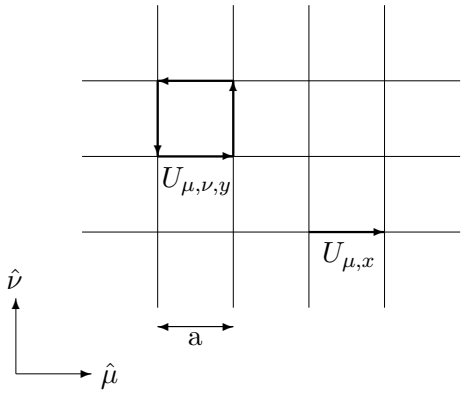

Figure 1: Basic building blocks of lattice Yang-Mills theory in 2 dimensions.

As a last step we need to define a lattice action. There are several ways to do this which may differ by their convergence behavior towards the continuum limit. This could, for example, mean that one of them matches the continuum action up to the order of a^2 while another one agrees with it up to even higher powers of the lattice spacing. Here we use the simplest variant as it suffices for our purposes. It is defined through elementary plaquette variables

$$U_{\mu,\nu,x} := U_{\mu,x}U_{\nu,x+a\hat{\mu}}U_{-\mu,x+a\hat{\mu}+a\hat{\nu}}U_{-\nu,x+a\hat{\nu}}, \tag{2.10}$$

where

$$U_{-\mu,x+a\hat{\mu}} = U^\dagger_{\nu,x}. \tag{2.11}$$

An elementary plaquette is a closed loop around a square of four nearest neighbor points as depicted in figure 1. Then the action takes the form

$$S[U] = -\frac{1}{4g_s^2}\sum_{x,\mu>\nu}\mathrm{Re}(\mathrm{tr}\, U_{\mu,\nu,x}), \tag{2.12}$$

where the sum is such that every plaquette occurs exactly once. This quantity is gauge invariant because of the cyclicity of the trace. In the continuum limit this yields the correct results up to the order of a^2. Then $\sum_{\mu>\nu} a^4$ is replaced by $\frac{1}{2}\int d^4x$ (which actually implies that we have to calculate up to order a^4 thereby making the calculation somewhat tedious).

To summarize, the partition function in the lattice regularization takes the form

$$Z = \prod_{\mu,x}\int_{SU(N)} DU_{\mu,x}\, \exp(-S[U]), \quad S[U] = -\frac{1}{4g_s^2}\sum_{x,\mu>\nu}\mathrm{Re}(\mathrm{tr}\, U_{\mu,\nu,x}), \tag{2.13}$$

which is completely well defined once one introduces the so-called Haar measure on the group space of $SU(N)$.

2.1.1. The Haar measure

The Haar measure is the gauge invariant measure on a gauge group. Mathematically it is the unique measure dU on a compact group G which obeys [11]

1. **Invariance:** $\int_G dU\, f(U) = \int_G dU\, f(VU) = \int_G dU\, f(UV) \quad \forall V \in G$,
2. **Normalization:** $\int_G dU = 1$.

It is a generalization of the Lebesgue measure on $\mathbb{R}^n$ and has the properties

$$\int_{SU(N)} dU\, U_{ij} = 0, \tag{2.14}$$

$$\int_{SU(N)} dU\, U_{ij} U^*_{kl} = \frac{1}{N}\delta_{ik}\delta_{jl}, \tag{2.15}$$

as can be easily verified e.g. for $SU(2)$ by noting that the integral over $SU(2)$ can be replaced by an integral over the unit sphere $S^3 = \{U_\mu \in \mathbb{R}^4 : |U| = 1\}$ if one identifies the two spaces by writing

$$U = U_0 \mathbf{1} + i\vec{U}\cdot\vec{\sigma}, \qquad U_0^2 + |\vec{U}|^2 = 1, \tag{2.16}$$

where $\mathbf{1}$ is the two-dimensional unit-matrix, $U_0 \in \mathbb{R}$, $\vec{U} \in \mathbb{R}^3$ and $\vec{\sigma} = (\sigma_1, \sigma_2, \sigma_3)$ are the three Pauli matrices.

2.2. Static quarks

From here on we will set the lattice spacing $a = 1$ to simplify the notation in the calculations. Before calculating anything, we first have to introduce the last missing piece: We need a representation for infinitely heavy quarks. The way to do this is by introducing the so-called Polyakov loop. Writing $x_4 = it$ for the (imaginary) Euclidean time direction it is defined as

$$\Phi_{\vec{x}} = \mathrm{tr}\left(\prod_{x_4=1}^{\beta} U_{4,(\vec{x},x_4)}\right) = \mathrm{tr}\left(U_{4,(\vec{x},1)}U_{4,(\vec{x},2)}U_{4,(\vec{x},3)}...U_{4,(\vec{x},\beta)}\right), \tag{2.17}$$

which in the continuum limit becomes

$$\Phi(\vec{x}) = \mathcal{P}\exp\left(\int_0^\beta dx_4\, G_4(\vec{x}, x_4)\right), \tag{2.18}$$

where $\mathcal{P}$ denotes path ordering and is defined through taking the continuum limit of the lattice based definition. Furthermore, the inverse temperature $\beta = \frac{1}{T}$ is the extent of the Euclidean time direction on a finite lattice with periodic boundary conditions in Euclidean time.

The Polyakov loop has a fixed spatial coordinate $\vec{x}$ as it extends only in the Euclidean time direction as depicted in figure 2. In fact, it is a closed loop in time, gauge invariant (as any physical quantity needs to be) and its expectation value,

$$\langle\Phi_{\vec{x}}\rangle = \frac{1}{Z}\prod_{\mu,x}\int_{SU(3)} DU_{\mu,x}\, \Phi_{\vec{x}} \exp(-S[U]) = \exp(-\beta F), \tag{2.19}$$

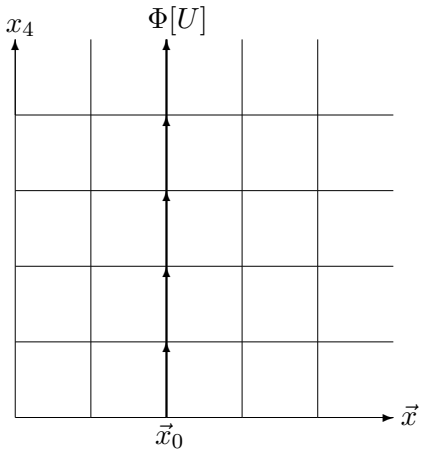

Figure 2: Polyakov loop at $\vec{x}_0$ on a lattice with periodic boundary conditions in Euclidean time.

is a measure of the free energy F of a static quark, i.e. the energy needed to add an additional static quark into the system of dynamical gluons at finite temperature T [9]. The Polyakov loop is an order parameter that distinguishes between confinement and deconfinement: In the confined phase it costs infinite energy to add a single quark which means that F is infinite and $\langle \Phi_{\vec{x}} \rangle = 0$. In the deconfined phase, on the other hand, single quarks cost a finite amount of energy. Therefore $F < \infty$ and $\langle \Phi_{\vec{x}} \rangle \neq 0$.

2.2.1. Area law for a quark-anti-quark pair

Using the Haar measure it is possible to do calculations in the strong coupling limit, i.e. by taking $g_s \to \infty$. To investigate confinement we are interested in expectation values of static quarks. Therefore we first calculate the expectation value of the Polyakov loop of a quark-anti-quark pair, i.e.

$$\langle \Phi_{\vec{x}} \Phi^*_{\vec{y}} \rangle = \frac{1}{Z} \prod_{\mu,z} \int_{SU(3)} DU_{\mu,z}\, \Phi_{\vec{x}} \Phi^*_{\vec{y}} \exp(-S[U]), \tag{2.20}$$

as shown in figure 3a. This can be calculated explicitly to first non-vanishing order in $\frac{1}{g_s^2}$ using eqs. (2.14) and (2.15): First we can simplify the expectation value using the strong

coupling limit,

$$\begin{aligned}
\langle \Phi_{\vec{x}} \Phi^*_{\vec{y}} \rangle &= \frac{1}{Z} \prod_{\mu,z} \int_{SU(3)} DU_{\mu,z}\, \Phi_{\vec{x}} \Phi^*_{\vec{y}} \exp(-S[U]) \\
&= \frac{1}{Z} \prod_{\mu,z} \int_{SU(3)} DU_{\mu,z}\, \Phi_{\vec{x}} \Phi^*_{\vec{y}} \exp\left(\frac{1}{4g_s^2} \sum_{x,\mu>\nu} \mathrm{Re}(\mathrm{tr}\, U_{\mu,\nu,x}) \right) \\
&= \frac{1}{Z} \prod_{\mu,z} \int_{SU(3)} DU_{\mu,z}\, \Phi_{\vec{x}} \Phi^*_{\vec{y}} \prod_{x,\mu>\nu} \exp\left(\frac{1}{4g_s^2} \mathrm{Re}(\mathrm{tr}\, U_{\mu,\nu,x}) \right) \\
&= \frac{1}{Z} \prod_{\mu,z} \int_{SU(3)} DU_{\mu,z}\, \Phi_{\vec{x}} \Phi^*_{\vec{y}} \prod_{x,\mu>\nu} \left(1 + \frac{1}{4g_s^2} \mathrm{Re}(\mathrm{tr}\, U_{\mu,\nu,x}) + O(\frac{1}{g_s^4}) \right) \\
&= \frac{1}{Z} \prod_{\mu,z} \int_{SU(3)} DU_{\mu,z}\, \Phi_{\vec{x}} \Phi^*_{\vec{y}} \prod_{x,\mu>\nu} \left(1 + \frac{1}{8g_s^2} (\mathrm{tr}\, U_{\mu,\nu,x} + \mathrm{tr}\, U^*_{\mu,\nu,x}) + O(\frac{1}{g_s^4}) \right). \quad (2.21)
\end{aligned}$$

Eq. (2.14) implies that every link for which there are more variables $U_{\mu,x}$ in one direction than variables $U_{-\mu,x+\hat{\mu}}$ in the opposite direction, this integral vanishes. Therefore the whole contribution of this configuration to the expectation value vanishes if we have any such links. In the last formula above we have plaquettes $\mathrm{tr}\, U_{\mu,\nu,x}$ and anti-plaquettes $\mathrm{tr}\, U^*_{\mu,\nu,x}$ to choose from, i.e. we can use those to counter the Polyakov loops as depicted in figure 3b. However, doing this just shifts the problem because we still create two rows of single variables as shown in figure 3c. The complete solution therefore is to tile up the space between the two Polyakov loops with plaquettes as in figure 3d. As every plaquette yields a factor proportional to g_s^{-2} this is also the first non-vanishing term in the strong coupling expansion,

$$\langle \Phi_{\vec{x}} \Phi^*_{\vec{y}} \rangle = \frac{N_p}{Z} \left(\frac{1}{8g_s^2} \right)^{R\beta} \frac{1}{N^{2R\beta+\beta}} + O(g_s^{-(A+2)}) = \frac{N_p}{ZN^\beta} \left(\frac{1}{8g_s^2 N^2} \right)^{R\beta} + O(g_s^{-(A+2)}), \quad (2.22)$$

where $R = |\Delta x_1 + \Delta x_2 + \Delta x_3|$ is the spatial distance between the Polyakov loops on the lattice, N_p is the number of shortest paths between x and y (which only depends on the number of lattice dimensions) and β is the extent of the Euclidean time direction. We then define

$$\langle \Phi_{\vec{x}} \Phi^*_{\vec{y}} \rangle \sim \exp(-\sigma A), \quad (2.23)$$

where A is the area between the two Polyakov loops, i.e. we have $A = R\beta$. If the expectation value behaves like this, it obeys an area law (because it decreases exponentially with the area between the loops). With the approximation above we can read off the string tension

$$\sigma = \ln(8N^2 g_s^2). \quad (2.24)$$

The area law implies confinement because for large separations between the quark and the anti-quark, i.e. for large R, the expectation value goes to zero. Therefore it is impossible to separate the quarks completely (to let R go to infinity).

The same calculation with just one Polyakov loop trivially leads to $\langle \Phi_x \rangle = 0$. As a consequence of eq. (2.15) there is no way to counter the link variables from the Polyakov loop using only plaquettes. Therefore, together with eq. (2.19), this shows that it is impossible to add a single static quark as it would require infinite energy. This shows that confinement indeed exists in the strong coupling limit of QCD. The other extreme case of vanishing coupling ($g_s \to 0$) is obviously deconfinement because it describes a free theory without interaction. This means that there must be a transition between these two phases.

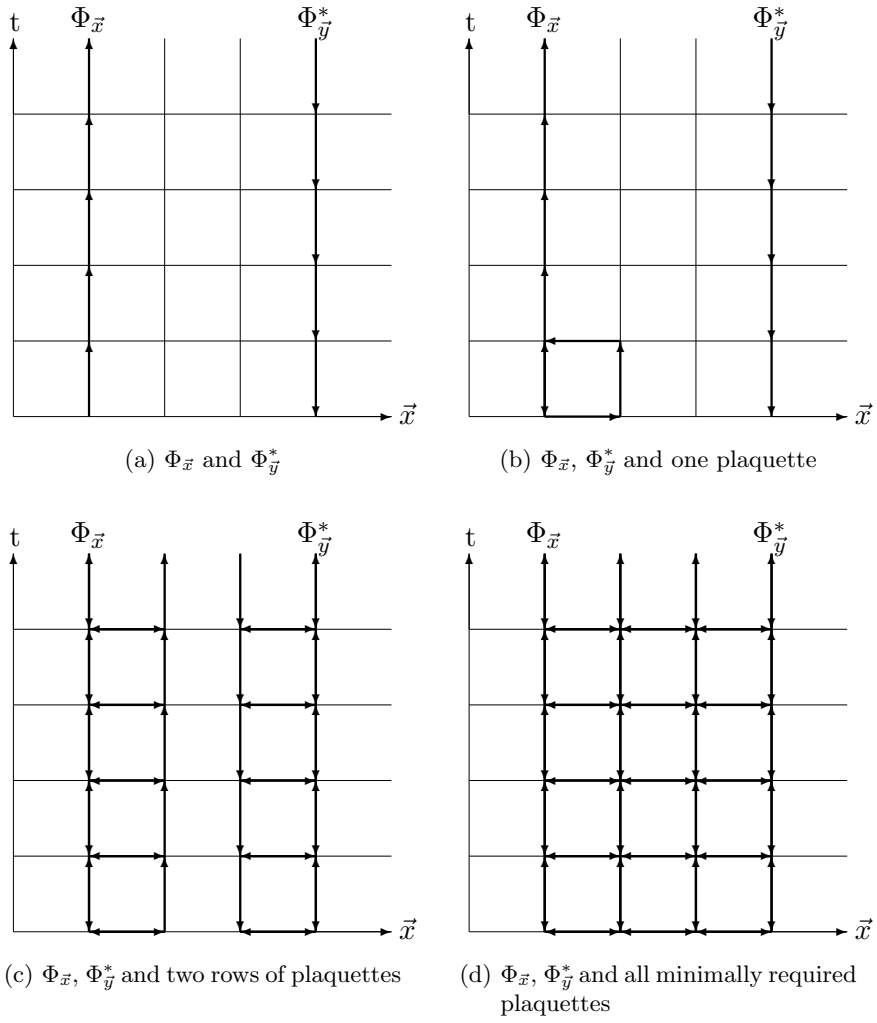

(a) $\Phi_{\vec{x}}$ and $\Phi^*_{\vec{y}}$

(b) $\Phi_{\vec{x}}$, $\Phi^*_{\vec{y}}$ and one plaquette

(c) $\Phi_{\vec{x}}$, $\Phi^*_{\vec{y}}$ and two rows of plaquettes

(d) $\Phi_{\vec{x}}$, $\Phi^*_{\vec{y}}$ and all minimally required plaquettes

Figure 3: Polyakov loop - anti-Polyakov loop pair

2.3. The center symmetry

Another way to look at confinement is using the center symmetry which is broken in the deconfined phase but unbroken in the confined phase [8].

The center $Z(G)$ of a group G is defined as the set of all elements which commute with every other group element, i.e.

$$Z(G) := \{z \in G : az = za \, \forall a \in G\}. \tag{2.25}$$

As can be easily verified, the center forms a subgroup of G. Here we are interested in the groups $SU(N)$, for which the center is equal to

$$Z(SU(N)) = \mathbb{Z}(N) := \mathbb{Z}/N\mathbb{Z} = \{\mathbf{1} \exp\left(\frac{2\pi i n}{N}\right) : n \in \{1, 2, ..., N\}\}, \tag{2.26}$$

where $\mathbf{1}$ is the $N \times N$ unit-matrix. We have assumed the standard representation of $SU(N)$ using complex N-dimensional matrices. Using this we can define a global center transformation of the fields by allowing gauge transformations with periodic boundary conditions up to

an element of the center in the Euclidean time direction, i.e. for gauge transformations Ω_x with

$$\Omega_{(\vec{x},\beta)} = z\Omega_{(\vec{x},0)}, \quad z \in Z(SU(N)). \tag{2.27}$$

In order to simplify studying this transformation we can use the fact that lattice Yang-Mills theory is gauge invariant. This means that we can actually omit the part of the transformation which consists of a gauge transformation and only keep the additional z factor. This is the same as multiplying each link variable on one time slice with z. For example we can define

$$U'_{\mu,(\vec{x},x_4)} := \begin{cases} U_{\mu,(\vec{x},x_4)} & x_4 \neq 0 \\ zU_{\mu,(\vec{x},0)} & x_4 = 0 \end{cases}, \quad z \in Z(SU(N)). \tag{2.28}$$

Figure 4 shows the links which get transformed in this case. Under these transformations the theory behaves as

$$S[U]' = S[U], \tag{2.29}$$

$$Z' = Z, \tag{2.30}$$

$$\Phi[U]' = \Phi[zU] = \Phi\left[\mathbf{1}\exp\left(\frac{2\pi i n}{3}\right)U\right] = \exp\left(\frac{2\pi i n}{3}\right)\Phi[U]. \tag{2.31}$$

Therefore in the pure gauge case, the center transformation is a symmetry of the theory. The Polyakov loop, however, is not invariant. This then implies the following: If we have $\langle\Phi\rangle = 0$, the factors from the Polyakov loop generated by the center transformation average out and the system remains invariant. On the other hand, if we have $\langle\Phi\rangle \neq 0$, the symmetry is spontaneously broken because the system is no longer invariant under center transformations. Therefore the realization of the center symmetry indicates whether the system is in a confined or a deconfined phase. This means that testing whether the symmetry is broken or not with a simulation tells us something about confinement. However, to only get some qualitative information about the transition it suffices to use a simplified model which shares the same symmetry. Therefore in the next chapter we will look at a model which preserves the center symmetry to further study confinement.

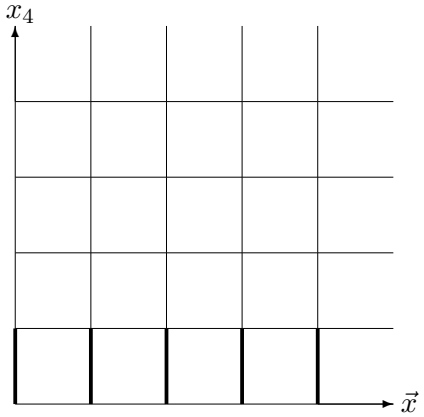

Figure 4: Center symmetry. The bold lines are an example of the links between points whose link variables $U_{\mu,x}$ get an additional factor $z \in \mathbb{Z}(N)$ from the center transformation.

3. The 3-d 3-state Potts model

3.1. Motivation and definition

As observed in the last chapter, studying the center symmetry tells us something about confinement. However, simulating Yang-Mills theory with static color charges is still rather difficult. Therefore we study here a simpler model. The 3-d 3-state Potts model has been used many times as an approximation to $SU(3)$ Yang-Mills theory [5, 3].

The model is defined in terms of Potts spins $\phi_x \in \mathbb{Z}(3)$ on each point of a 3-d spatial lattice without time direction. The action is replaced by a standard nearest neighbor Potts model interaction

$$S[\phi] = -\kappa \sum_{x,i} \delta_{\phi_x, \phi_{x+\hat{i}}}. \tag{3.1}$$

Here, κ qualitatively corresponds to the temperature of the system. Large κ equals large temperature (and not the other way around as in the standard statistical mechanics interpretation). In the lattice formulation, the partition function then becomes

$$Z = \prod_x \sum_{\phi_x \in \mathbb{Z}(3)} \exp(-S[\phi]), \tag{3.2}$$

where the sum and the product replace the integral over all configurations, i.e. they combine to a sum over all possible configurations. The model has a charge conjugation symmetry, i.e. the action is invariant under the transformation

$$\phi_x \to \phi_x^*. \tag{3.3}$$

The reason for using this model is that it also has another symmetry: It shares the $\mathbb{Z}(3)$ symmetry with Yang-Mills theory, i.e. it is invariant under transformations

$$\phi'_x = z\phi_x, \quad z \in \mathbb{Z}(3). \tag{3.4}$$

Moreover one could explicitly integrate out all degrees of freedom of the original path integral introduced in chapter 2 except for the center variables by writing it in terms of

$$\exp(-S_{\text{eff}}[z]) = \int_{SU(3)} \mathcal{D}U \exp(-S[U]) \prod_{\vec{x}} \delta_{z_{\vec{x}}, P(\phi_{\vec{x}})}, \tag{3.5}$$

where P is a projection operator from $SU(3)$ onto $\mathbb{Z}(3)$. With this we could write

$$Z = \prod_x \sum_{z_x \in Z(3)} \exp(-S_{\text{eff}}[z]), \tag{3.6}$$

which is equivalent to the standard Yang-Mills partition function because of the Kronecker-δ. The problem here is the calculation of S_{eff}. It is currently not possible to explicitly calculate this and if it were it would result in a rather complicated non-local action. Still, this shows that in principle one can turn Yang-Mills theory into a model with a $\mathbb{Z}(3)$ symmetry. If one further assumes that the nearest-neighbor interactions are the most important ones, then one arrives at a variant of the Potts model. Therefore it is a reasonable approximation to lattice Yang-Mills theory.

As has been explained in chapter 1, we want to examine an approximate model for Yang-Mills theory with a fixed finite number Q of static color charges. For reasons which get clearer below, we even restrict ourselves to a fixed baryon number $B = 3Q$. Each quark is represented by a Polyakov loop as has been explained before which simplifies to

$$\Phi[U] \to \phi_x \tag{3.7}$$

for a color charge at position x where the product over all time slices disappears from eq. (2.17) because the Potts model is a static model without time-direction. Therefore the full partition function can be written as

$$Z = \prod_x \sum_{\phi_x \in \mathbb{Z}(3)} \sum_{n_x=0}^{3} \exp(-S[\phi]) \delta_{\sum_x n_x, Q} \prod_x \phi_x^{n_x}, \tag{3.8}$$

where n_x is the number of quarks at position x. In general we could add different types of quarks representing the flavors of QCD. Also anti-quarks could be allowed which are described by ϕ_x^* instead of ϕ_x. However, for simplicity we don't consider these possibilities. We only allow to have up to three quarks per site x. This is because, on one hand, in full QCD we got three different colors which a quark can have but, on the other hand, the Pauli principle forbids more than one particle of the same species at the same point. Therefore we only allow $n_x = 0, 1, 2, 3$.

3.2. The Potts model without quarks

If we set all n_x equal to 0, we get the standard 3-d 3-state Potts model. It doesn't have any kind of complex action problem, wherefore it can be simulated using a standard Metropolis algorithm, i.e. in each step we randomly choose a new value $\phi_x \in \mathbb{Z}(3)$ for a point x and accept this new configuration with probability

$$p = \min\{1, \exp(-\Delta S)\} = \min\{1, \exp(-(S_{\text{new}} - S_{\text{old}}))\}. \tag{3.9}$$

Doing this, however, leads to a subtle problem: For large κ (or equivalently for large temperatures) the convergence is very slow. That is because then (almost) every point has the same value $\phi_0 \in \mathbb{Z}(3)$ and it is extremely improbable to change into a configuration where every point has the value $\phi_1 \neq \phi_0$, even though its Boltzmann weight is the same. If we represent the $\mathbb{Z}(3)$ values as complex numbers, i.e.

$$\mathbb{Z}(3) = \left\{ \mathbf{1} \exp\left(\frac{2\pi i n}{3}\right) : n \in \{0, 1, 2\} \right\}, \tag{3.10}$$

then we can use the observable

$$\left\langle \text{Im} \frac{1}{V} \sum_x \phi_x \right\rangle \tag{3.11}$$

to show this behavior because all three Potts spin values have a different imaginary part $(0, \pm\frac{\sqrt{3}}{2})$. Figure 5 shows a plot of this using the Metropolis algorithm. Even though the algorithm is in principle ergodic, the system obviously stays in a configuration where all spins have the same value ($-\frac{\sqrt{3}}{2}$ in this case) which is not correct as the other two possibilities

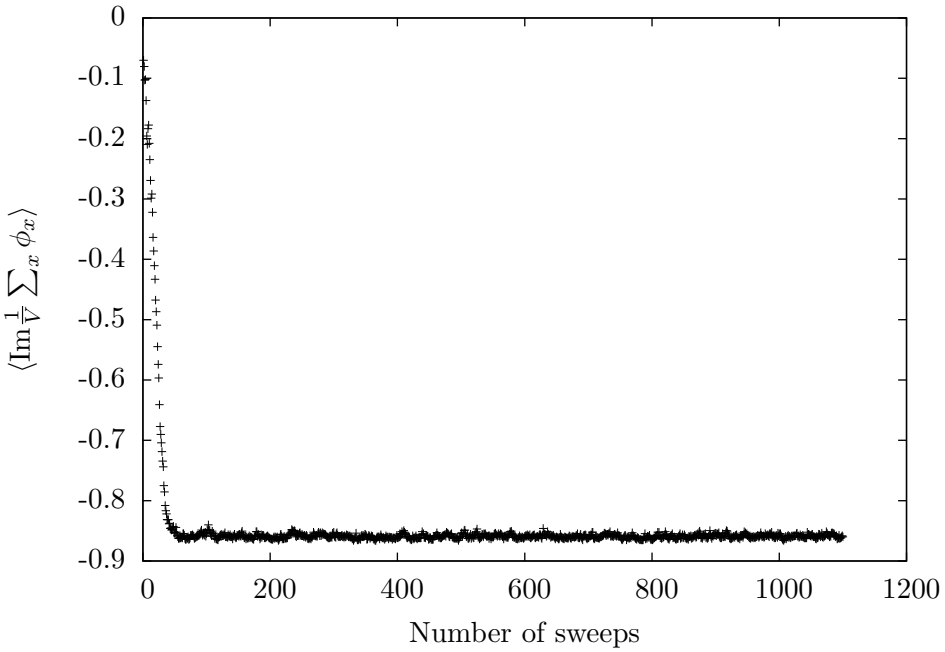

Figure 5: Problem of the Metropolis algorithm for the Potts model.

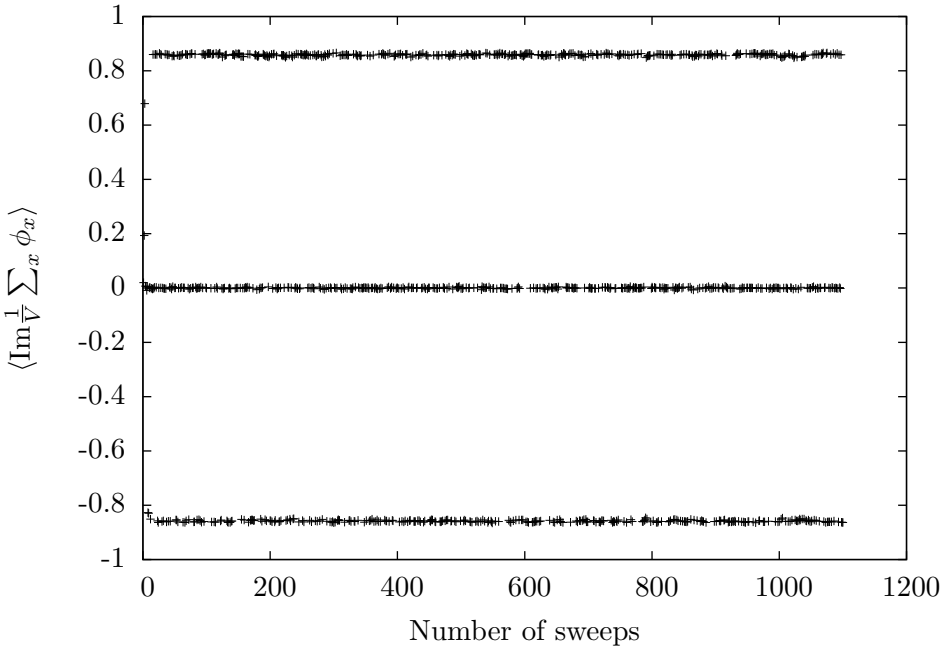

Figure 6: The cluster algorithm solves the problem of the Metropolis algorithm for the Potts model.

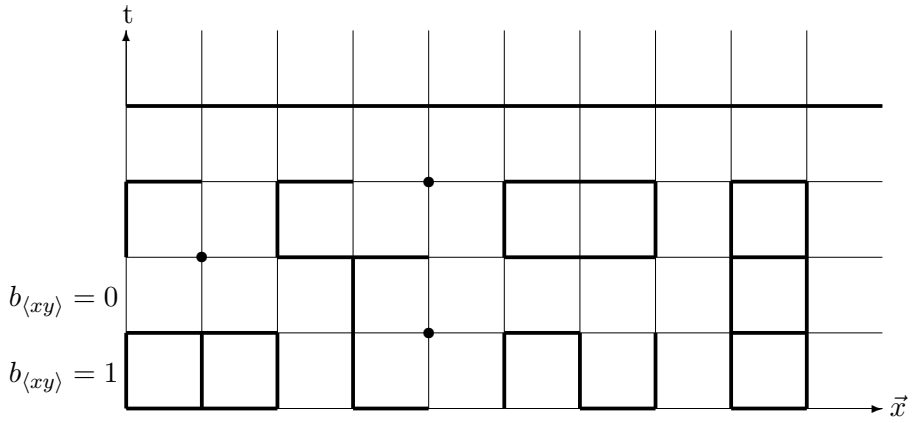

Figure 7: Example distribution of bonds and 10 clusters (including the 3 single-site clusters depicted by dots) defined by connected activated bonds.

actually have the same Boltzmann weight $\exp(-S)$ and should therefore appear as often. Solving this requires using a better algorithm, in our case we used a cluster algorithm. It manages to avoid this problem as figure 6 clearly shows.

The main difference between the Metropolis and the cluster algorithm is that in the latter, in general, we don't switch the value of only one point at once anymore. Instead we form clusters of points with equal values and then switch those all together. To do this we first introduce bond variables $b_{\langle xy\rangle} = 0, 1$ for each link connecting two neighboring lattice sites x and y. A sweep then consists of the following steps:

1. **Put bonds:** Visit each bond and activate the bond with probability $p_b := 1 - \exp(-\kappa)$ (see below), if the two connected sites have the same spin value. Otherwise deactivate it.

2. **Identify clusters:** A cluster is defined as a set of all points connected via activated bonds. Every site not connected to any other site via activated bonds forms its own single site cluster.

3. **Switch cluster values:** For each cluster, randomly decide on a new spin value giving each of the three possibilities the same probability.

An example configuration of bonds and clusters is given in figure 7.

The probability p_b can be calculated as follows [1]: We rewrite the factor of the action for a bond as

$$\exp(\kappa\delta_{\phi_x,\phi_y}) = \sum_{b_{\langle xy\rangle}=0}^{1} \left[\delta_{b_{\langle xy\rangle},1}\delta_{\phi_x,\phi_y}(\exp(\kappa) - 1) + \delta_{b_{\langle xy\rangle},0}\right] \tag{3.12}$$

where $y = x+\hat{i}$ is the neighbor of x in a given direction i. From this we see that the Boltzmann weight of an active bond is $W_{b_{\langle xy\rangle}=1} = \delta_{\phi_x,\phi_y}(\exp(\kappa) - 1)$, the weight for a deactivated bond is $W_{b_{\langle xy\rangle}=0} = 1$. Assuming $\phi_x = \phi_y$, we can then calculate the probability to put a bond

$$p_b = \frac{W_{b_{\langle xy\rangle}=1}}{W_{b_{\langle xy\rangle}=1} + W_{b_{\langle xy\rangle}=0}} = \frac{\delta_{\phi_x,\phi_y}(\exp(\kappa) - 1)}{\delta_{\phi_x,\phi_y}(\exp(\kappa) - 1) + 1} = \frac{\exp(\kappa) - 1}{\exp(\kappa)} = 1 - \exp(-\kappa). \tag{3.13}$$

As this result is directly based on the probability distribution of the Metropolis algorithm, detailed balance is also fulfilled for the cluster algorithm. Ergodicity is satisfied as well since it is possible to generate every allowed configuration of the lattice. Starting e.g. from a configuration where every spin has the same value, every bond can individually be put or not, thereby (in principle) generate every possible cluster configuration with a non-vanishing probability. Realizing every cluster configuration is obviously equivalent to generating every spin value configuration. Detailed balance additionally ensures that the reverse path is possible as well. Together this implies that every configuration is reachable from every other configuration with a non-zero probability, i.e. ergodicity is indeed fulfilled.

Apart from solving the efficiency problem, the cluster algorithm also has other advantages: We can now construct improved estimators of certain observables by analytically averaging over Potts spin values. The magnetization for example can be rewritten using

$$\sum_x \phi_x = \sum_{C_i \in C} \sum_{x \in C_i} \phi_x = \sum_{C_i \in C} |C_i| \phi_{C_i}, \tag{3.14}$$

where C is the set of all clusters and $|C_i|$ is the size of the cluster C_i, i.e. the number of sites it contains. In the last equality we used that every site in a cluster C_i has the same value ϕ_{C_i}. The magnetization then becomes

$$\chi = \left\langle |\sum_x \phi_x|^2 \right\rangle = \left\langle \sum_x \sum_y \phi_x \phi_y^* \right\rangle = \left\langle \sum_{C_i \in C} \sum_{C_j \in C} |C_i||C_j| \phi_{C_i} \phi_{C_j}^* \right\rangle = \left\langle \sum_{C_i \in C} |C_i|^2 \right\rangle, \tag{3.15}$$

where we used that the product $\phi_{C_i}\phi_{C_j}^*$ adds up to zero for $C_i \neq C_j$ if we average over the three values of $\mathbb{Z}(3)$ (because $\sum_{z \in \mathbb{Z}(3)} z = 0$). This means that we can analytically evaluate some of the other configurations with the same Boltzmann weight which implies that we will have a smaller statistical error as it increases our statistics (we considered more different configurations than before and averaged over them).

The cluster algorithm in this form is rather efficient even though it still slows down near the phase transition. This is because then the confined and the deconfined phases coexist and switching between those is inefficient. Nevertheless it can be used to study the phase transition of the Potts model without quarks. We used χ and the expectation value of the action $\langle S \rangle = \langle -\kappa \sum_{x,i} \delta_{\phi_x, \phi_{x+\hat{i}}} \rangle$ as observables to determine the value of the coupling constant κ_T at the point of the phase transition using the methods which will be explained in chapter 5. Doing this we were able to reproduce the value of $\kappa_T \approx 0.5506$ known from the literature [1, 4].

3.3. Adding quarks to the model

3.3.1. Complex action problem and its solution

As mentioned above, the Potts model with a fixed number of quarks is defined through its partition function

$$Z = \prod_x \sum_{\phi_x \in \mathbb{Z}(3)} \sum_{n_x=0}^{3} \exp(-S[\phi]) \delta_{\sum_x n_x, Q} \prod_x \phi_x^{n_x}. \tag{3.16}$$

If not all the n_x are equal to zero, then this model suffers from a complex action problem. In general the factors $\phi_x^{n_x}$ are then complex numbers which cannot be interpreted as a probability

distribution. This would stop us from using it as a Boltzmann weight. A possible solution for this is to still use $\exp(-S)$ as a probability density and move the complex phase into the observables. This means that for an observable $\mathcal{O}$ instead of $\langle\mathcal{O}\rangle$ we had to evaluate

$$\langle\mathcal{O}\rangle' = \frac{\langle\mathcal{O}\prod_x \phi_x^{n_x}\rangle}{\langle\prod_x \phi_x^{n_x}\rangle}. \tag{3.17}$$

This quantity however would suffer from serious cancellation problems and its simulation would be extremely inefficient. To explain this we write

$$\exp(i\varphi) := \prod_x \phi_x^{n_x}, \tag{3.18}$$

which is well-defined because $|\phi_x| = 1$ and therefore $|\prod_x \phi_x^{n_x}| = 1$. We can then calculate

$$\langle\exp(i\varphi)\rangle_a = \frac{1}{Z_a}\sum_c \exp(-S)\exp(i\varphi) = \frac{Z}{Z_a} = \frac{\exp(-\beta f V)}{\exp(-\beta f_a V)} = \exp(-\beta\Delta f V). \tag{3.19}$$

This quantity gets very small for large inverse temperatures β and/or large volumes V. Therefore, in these cases, both the nominator and the denominator of eq. (3.17) get small. However the ratio between the two quantities is of order 1. A small change in $\langle\prod_x \phi_x^{n_x}\rangle$ then implies a large change in $\langle\mathcal{O}\rangle'$. We therefore need to have a very small error of $\langle\prod_x \phi_x^{n_x}\rangle$ in order to obtain a decent accuracy of $\langle\mathcal{O}\rangle'$ (a somewhat more detailed explanation of this can be found e.g. in [1] for a slightly different model). This is practically impossible, making this solution rather useless.

A better way is to directly solve the whole problem by rewriting the model in such a way that we don't have a complex action anymore. To do this we can use a mathematical statement which says

$$\forall x \in G \,:\, x^{|G|} = 1, \tag{3.20}$$

where G is an arbitrary finite group and $|G|$ is the number of elements in this group. In our case this translates to the fact that

$$\phi^3 = 1 \quad \forall\phi \in \mathbb{Z}(3). \tag{3.21}$$

If we would rewrite the Potts model in terms of bond variables and clusters only instead of the Potts spins, we could ensure that within each cluster we have a multiple of three quarks. This is reasonable because if we have a cluster with one or two quarks (modulo 3), these configurations actually don't contribute to the partition function. The reason is that if we have one quark (modulo 3) all the three values of it are, in fact, equally probable and therefore we get no contribution from them because $\sum_{z\in\mathbb{Z}(3)} z = 0$. Having two quarks (modulo 3) in a cluster doesn't change this result because then we have a Potts value squared which is still a value of $\mathbb{Z}(3)$ and in general different from one. Therefore the same reasoning applies. For zero quarks (modulo 3) the factor contributed by these quarks becomes one and therefore the whole product,

$$\prod_x \phi_x^{n_x} = \prod_{C_i\in C} \phi_{C_i}^{n_{C_i}} = 1, \tag{3.22}$$

would vanish from our partition function thereby solving the complex action problem completely.

To be able to make use of this observation we first rewrite the partition function:

$$\begin{aligned} Z &= \prod_x \sum_{\phi_x \in \mathbb{Z}(3)} \sum_{n_x=0}^{3} \exp(-S[\phi]) \delta_{\sum_x n_x, Q} \prod_x \phi_x^{n_x} \\ &= \prod_x \sum_{\phi_x \in \mathbb{Z}(3)} \sum_{n_x=0}^{3} \exp(-S[\phi]) \delta_{\sum_x n_x, Q} \underbrace{\prod_{C_i \in C} \phi_{C_i}^{n_{C_i}}}_{=1} \\ &= \prod_{b_{\langle xy \rangle}} \sum_{b_{\langle xy \rangle}=0}^{1} \sum_{n_x=0}^{3} W[b] 3^{|C_{[b]}|} \delta_{\sum_x n_x, Q}, \end{aligned} \tag{3.23}$$

where the first product is over all bonds, $|C_{[b]}|$ is the number of clusters of the configuration $[b]$ and $W[b]$ is its Boltzmann factor,

$$W[b] := \prod_{b_{\langle xy \rangle}} \left(\delta_{b_{\langle xy \rangle},1} (\exp(\kappa) - 1) + \delta_{b_{\langle xy \rangle},0} \right). \tag{3.24}$$

The factor $3^{|C_{[b]}|}$ in the last line of eq. (3.23) comes from averaging over the three values of the Potts spins of a given cluster. Using the fact that the factor $\delta_{b_{\langle xy \rangle},0}$ can be neglected in the product (because it is either not there or equal to one), the partition function can also be written as

$$Z = \prod_{b_{\langle xy \rangle}} \sum_{b_{\langle xy \rangle}=0}^{1} \sum_{n_x=0}^{3} W(\kappa)^{n_b} 3^{|C_{[b]}|} \delta_{\sum_x n_x, Q}, \tag{3.25}$$

where $W(\kappa) = \exp(\kappa) - 1$. Here $n_b := \sum_{b_{\langle xy \rangle}} b_{\langle xy \rangle}$ is the number of activated bonds.

Using this representation we can then define a modified version of the cluster algorithm for the Potts model without quarks. We start from an arbitrary configuration of bonds (and therefore also of clusters). Then a sweep consists of the following steps:

1. **Update bonds:** For each bond, decide whether to change it according to:
   - If the bond is not activated and both neighboring points are already part of the same cluster, then activate the bond with probability $p = \min\{1, \exp(\kappa) - 1\}$.
   - If the bond is activated and the clusters of the neighboring points are different, then activate the bond with probability $p = \min\{1, \frac{\exp(\kappa)-1}{3}\}$ (the factor 3 comes from $3^{|C_{[b]}|}$ in the partition function because afterwards we have one cluster less).
   - If the bond is already activated and after removing the bond the cluster would not decay into two disconnected parts, then deactivate the bond with probability $p = \min\{1, \frac{1}{\exp(\kappa)-1}\}$.
   - If the bond is activated and its removal splits the cluster in two, then verify that both clusters have a multiple of three quarks. If this is true, then deactivate the bond with probability $p = \min\{1, \frac{3}{\exp(\kappa)-1}\}$. Otherwise do nothing.

2. **Update quarks:** For each cluster C_i, move the quarks in it randomly, i.e. randomly choose two sites $x, y \in C_i$. If x has quarks and y has less than three quarks, then move one quark from x to y.

These steps yield a correct Monte Carlo algorithm because both ergodicity and detailed balance are fulfilled. Ergodicity for the clusters is satisfied because, in principle, every combination of clusters is reachable. For the quarks this means that moving them within one cluster ensures that they can change clusters (via cluster splitting) and therefore reach every site. Also detailed balance poses no problem as we essentially use the same probabilities as before. Therefore this algorithm together with the rewriting completely solves the complex action problem of the Potts model with static quarks.

3.3.2. Observables and meron-clusters

Calculating the expectation value of observables with the above algorithm is in principle possible. However, the ones we used, namely the action $\langle S \rangle$ and the susceptibility χ both need some adjustments in either their definition or in the algorithm itself. The action we have defined before was written in terms of the Potts variables,

$$S = -\kappa \sum_{x,i} \delta_{\phi_x, \phi_{x+\hat{i}}}. \tag{3.26}$$

In the reformulated model, however, the Potts spins are completely replaced by bond variables, wherefore we need to change this definition. As can easily be checked, an equivalent definition of the expectation value of the action is

$$\langle S \rangle = -\kappa \frac{\partial \log Z}{\partial \kappa}. \tag{3.27}$$

This formula doesn't refer to the Potts variables. Therefore it is still valid in the rewritten model and we can calculate the action using the representation of eq. (3.25) of the partition function,

$$\begin{aligned} \langle S \rangle = -\kappa \frac{\partial \log Z}{\partial \kappa} &= -\kappa \frac{1}{Z} \prod_{b_{\langle xy \rangle}} \sum_{b_{\langle xy \rangle}=0}^{1} \sum_{n_x=0}^{3} \frac{\partial W(\kappa)^{n_b}}{\partial \kappa} 3^{|C_{[b]}|} \delta_{\sum_x n_x, Q} \\ &= \frac{1}{Z} \prod_{b_{\langle xy \rangle}} \sum_{b_{\langle xy \rangle}=0}^{1} \sum_{n_x=0}^{3} \frac{-\kappa n_b}{W(\kappa)} W(\kappa)^{n_b} 3^{|C_{[b]}|} \\ &= \left\langle \frac{-\kappa n_b}{1 - \exp(-\kappa)} \right\rangle. \end{aligned} \tag{3.28}$$

This new representation can easily be evaluated using the above algorithm.

The expectation value for the susceptibility χ suffers a priori from a different problem:

$$\chi = \sum_x \sum_y \langle \phi_x \phi_y^* \rangle \tag{3.29}$$

contains a product of a quark at position x (ϕ_x) and an anti-quark at y (ϕ_y^*). Therefore the constraint of having a multiple of three quarks per cluster needs to be modified:

- If x and y are not part of the same cluster, then the cluster containing x is only allowed to have $2+3n$ quarks ($n \in \mathbb{N}$) apart from ϕ_x, the one containing the site y needs $1+3m$ ($m \in \mathbb{N}$).
- If x and y are part of the same cluster, nothing changes.

In order to handle this in the simulation, let us introduce the concept of a meron-cluster similar to what has been done in [3]. A meron-cluster is a cluster with one missing quark, i.e. one with $2+3n$ ($n \in \mathbb{N}$) quarks. An anti-meron is one with one additional quark, i.e. one with $1+3m$ ($m \in \mathbb{N}$) quarks. As can be easily verified, the Potts model with a fixed number of baryons always has an equal number of meron and anti-meron clusters.

With these definitions we can now speak of the zero-meron sector with neither meron nor anti-meron clusters and of the two-meron sector with exactly one meron and one anti-meron cluster. These are the only sectors relevant in this context. We now modify the algorithm in such a way that we visit both the zero-meron sector and the two-meron sector. The easiest way to achieve this is to modify the first step in the algorithm above to allow transitions into the two-meron sector. However, we have to adjust for the fact that the two-meron sector is much bigger than the zero-meron sector (every zero-meron sector configuration can be turned into several two-meron sector configurations by moving any quark into another cluster). Naively allowing all transitions into the two-meron sector would lead to spending a comparatively long time in the two-meron sector and only a small fraction in the zero-meron sector. The latter, however, gives the bigger contribution to χ (and also the expectation value of the action gets no contribution from the two-meron sector at all) as will be explained below. A possible solution for this problem is to make it less probable to actually enter the two-meron sector (and to correctly account for this when calculating the expectation values, see below), i.e. enter it only with probability p_2. Doing this changes the algorithm to:

1. **Update bonds:** For each bond, decide whether to change it according to:
   - If the bond is not activated and both neighboring points are already part of the same cluster, then activate the bond with probability $p = \min\{1, \exp(\kappa) - 1\}$.
   - If the bond is not activated and the clusters of the neighboring points are different, then activate the bond with probability $p = \min\{1, \frac{\exp(\kappa)-1}{3}\}$.
   - If the bond is already activated and after removing the bond the cluster would not decay into two disconnected parts, then deactivate the bond with probability $p = \min\{1, \frac{1}{\exp(\kappa)-1}\}$.
   - If the bond is activated and its removal splits the cluster in two, then verify that both clusters have a multiple of three quarks. If this is true, then deactivate the bond with probability $p = \min\{1, \frac{3}{\exp(\kappa)-1}\}$. Otherwise check if we would be in the two-meron sector. If so, accept this with probability $p = \min\{1, \frac{3p_2}{\exp(\kappa)-1}\}$. If none of this is the case, then do nothing.
2. **Update quarks:** For each cluster C_i, move the quarks in it randomly, i.e. randomly choose two sites $x, y \in C_i$. If x has quarks and y has less than three quarks, then move one quark from x to y.

These modifications don't actually change anything apart from allowing transitions between the two-meron and the zero-meron sector. Therefore ergodicity and detailed balance are still fulfilled even in this larger configuration space.

As mentioned above, the expectation value of the action only gets contributions form the zero-meron sector. This is because in the two-meron sector, when calculating the action, we don't have these additional quarks. Therefore the constraint is violated and we have a cluster with one additional quark and one with a missing quark. Averaging over the Potts spin values then leads to vanishing contributions of these configurations. This means that the expectation value of the action can be calculated as before, we just have to be careful to take only contributions from the zero-meron sector (and average it over the number of configurations generated in the zero-meron sector) while ignoring all configurations in the two-meron sector. This is another reason to introduce p_2, i.e. to make it less probable to be in the two-meron sector, because the more time we spend in the two-meron sector the less time is spent in the zero-meron sector. The result is then that we have less statistics for this observable. Therefore we need to have a way to balance between increased statistics for the susceptibility and for the expectation value of the action.

As mentioned above, the susceptibility χ receives contributions from the zero- and the two-meron sector. The zero-meron sector contributions are still the same as before, i.e. we just sum up the cluster sizes squared,

$$\chi_0 = \left\langle \sum_{C_i \in C} |C_i|^2 \right\rangle, \tag{3.30}$$

where the index 0 denotes contributions from the zero-meron sector. In the two-meron sector the contributions are different. Calculating the expectation value, we obtain

$$\chi_2 = \left\langle |\sum_x \phi_x|^2 \right\rangle = \left\langle \sum_x \sum_y \phi_x \phi_y^* \right\rangle = \left\langle \sum_{C_i \in C} \sum_{C_j \in C} |C_i||C_j| \phi_{C_i} \phi_{C_j}^* \right\rangle = \langle |C_1||C_2| \rangle, \tag{3.31}$$

where C_1 is the meron cluster and C_2 is the anti-meron cluster. The last equality follows because the average vanishes for every cluster except the ones where adding the quark or the anti-quark makes the number of quarks in this cluster a multiple of three, i.e. it vanishes for all clusters except the meron and the anti-meron cluster. If we denote the number of meron-clusters by N (i.e. $N = 0$ if we are in the zero-meron sector, $N = 2$ if we are in the two-meron sector), we can calculate the expectation value of the susceptibility [3] (note that the authors of this paper use somewhat different conventions than we use here)

$$\chi = \frac{\left\langle \sum_{C_i \in C} |C_i|^2 \delta_{N,0} + \frac{|C_1||C_2|}{p_2} \delta_{N,2} \right\rangle}{\langle \delta_{N,0} \rangle}. \tag{3.32}$$

From here on, the last thing to be done is getting a reasonable value for p_2. As it turns out, different p_2 lead to different results for the statistical error. As mentioned above, for the expectation value of the action this behavior is expected. For the susceptibility this is less obvious. Still, from the way the error analysis works (as explained in appendix A), we obtain the smallest error if both contributions (from the zero- and the two-meron sector) are of the same order. A more precise discussion of the effect on the statistical error of this so-called reweighting can e.g. be found in [7]. Finding a good value for this, however, is non-trivial and the only way we used was to try different values and to choose those leading to the smallest errors.

3.3.3. The two-meron sector problem

In principle, we now have everything to simulate the Potts model with static quarks. Doing this, however, doesn't quite work for a practical reason: As has been mentioned, the two-meron sector is much bigger than the zero-meron sector. With our approach we can restrict the probability with which to enter the former. However, if the system is already in the two-meron sector, we have no way of ensuring that we actually return to the zero-meron sector in a reasonable amount of time. This means that if the relative size difference between the sectors is too big, it is almost impossible to return to the zero-meron sector. While simulating the model, this is exactly the situation we encountered once the system entered the two-meron sector: It never returned to the zero-meron sector. Such a run then yields no useful results as it entered the two-meron sector generally after just a few sweeps. Then we didn't have enough statistics in the zero-meron sector leading to a bigger error (or, in the extreme case, even no sweeps in the zero-meron sector leading to not being able to actually calculate anything because the denominator in formula (3.32) vanishes). Not visiting the two-meron sector at all would be a possibility if we were only interested in calculating the expectation value of the action. However we also want to calculate the susceptibility because it shows the phase transition significantly better as will be shown in chapter 5. Therefore not visiting the two-meron sector is not an option for us. This means that we had to search for a different solution. We didn't find a way to circumvent this directly. However, using a flux model which is equivalent to the Potts model but doesn't suffer from this problem (and neither from the complex action problem), we found an even better solution which will be explained in the next chapter. This finding then led us to abandon the search for a solution of this problem within the Potts model itself though we still ensured that if we happen to avoid this problem (e.g. by simulating on a small lattice or by only calculating the expectation value of the action) our algorithms work and give the correct result.

4. Flux representation of the Potts model

4.1. Definition of the flux model

The flux model is defined in terms of flux variables $E_{x,i} \in \{-1, 0, 1\}$ on the links between neighboring points x and $x + \hat{i}$ and the number of charges $n_x \in \{0, 1, 2, 3\}$ at a point x. The flux variables are directed fluxes, i.e. $E_{x,i}$ is a flux flowing from point x in direction i. There exists also a flux conservation rule, a $\mathbb{Z}(3)$ Gauss law such that for each point we must have

$$n_x = \sum_i \left(E_{x,i} - E_{x-\hat{i},i} \right) \mod 3. \tag{4.1}$$

As in the Potts model, the action has a simple nearest-neighbor interaction, i.e.

$$S[E] = \frac{g^2}{2} \sum_{x,i} E_{x,i}^2 := g' \sum_{x,i} E_{x,i}^2, \tag{4.2}$$

where we defined g' as a shorthand notation for the factor $\frac{g^2}{2}$. With this action, the partition function can be written as

$$Z_f = \prod_x \sum_{n_x \in \{0,1,2,3\}} \prod_{x,i} \sum_{E_{x,i} \in \{0,\pm 1\}} \prod_x \delta_x \exp(-S[E]) \delta_{\sum_x n_x, Q}, \tag{4.3}$$

where δ_x ensures the Gauss law (4.1) and can be written as

$$\delta_x = \frac{1}{3} \sum_{\phi_x \in \mathbb{Z}(3)} \phi_x^{n_x - (\sum_i (E_{x,i} - E_{x-\hat{i},i})}. \tag{4.4}$$

This can be easily verified by noting that if the constraint is fulfilled, i.e. if

$$n_x - \sum_i (E_{x,i} - E_{x-\hat{i},i}) = 0 \mod 3, \tag{4.5}$$

we trivially get $\delta_x = 1$. Otherwise the sum adds up to zero because $\sum_{\phi_x \in \mathbb{Z}(3)} \phi_x = 0$.

From the definition it is clear, that the flux variables $E_{x,i}$ replace the Potts spins ϕ_x and the number of charges n_x represent the number of quarks as in the Potts model. Still there are some remarkable differences: For example, the action of the Potts model $S[\phi]$ is always less or equal to zero, i.e. $S[\phi] \leq 0$, while for the flux model we have $S[E] \geq 0$. This is significant as it actually implies that $\kappa \to 0$ corresponds to $g \to \infty$, i.e. in some sense the two models are dual to each other. The high temperature deconfined state in the flux model is characterized by having many closed loops, confinement corresponds to having only a few closed loops. Typical high and low temperature situations are shown in figures 8a and 8b, respectively, where arrows indicate fluxes $E_{x,i}$ (which are 1 if the arrow points in the positive direction and -1 if it points in the negative direction). A last point worth mentioning is that (as with the bond and cluster representation of the Potts model) we can't distinguish the three high temperature phases anylonger as they all look the same now. Therefore we don't need to worry about the problem we had with the original Metropolis algorithm which, in practice, didn't generate each of these phases the same number of times.

All these differences need to be accounted for when we want to obtain results for the Potts model using the flux model. This will be covered further below. First, however, we will show that the two models are in fact equivalent.

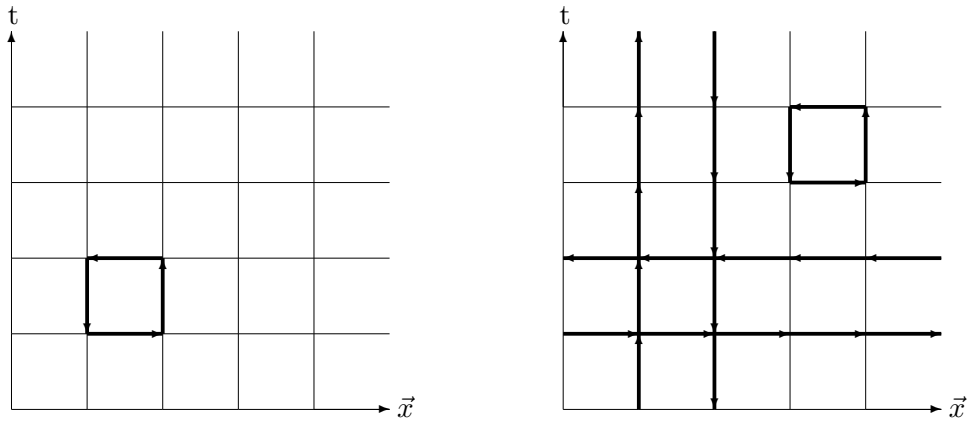

(a) Typical low temperature flux model configuration.

(b) Typical high temperature flux model configuration.

Figure 8: Typical flux model configurations.

4.2. Equivalence to the Potts model

Inserting the δ-function and the action into the partition function, we can simplify the equation,

$$\begin{aligned} Z_f &= \prod_x \sum_{n_x} \prod_{x,i} \sum_{E_{x,i}} \prod_x \frac{1}{3} \sum_{\phi_x \in \mathbb{Z}(3)} \phi_x^{n_x - (\sum_i (E_{x,i} - E_{x-\hat{i},i})} \exp\left(-g' \sum_{x,i} E_{x,i}^2\right) \delta_{\sum_x n_x, Q} \\ &= \prod_x \sum_{n_x} \prod_{x,i} \sum_{E_{x,i}} \prod_x \frac{1}{3} \sum_{\phi_x \in \mathbb{Z}(3)} \phi_x^{n_x} \left(\phi_x^* \phi_{x+\hat{i}}\right)^{E_{x,i}} \exp\left(-g' \sum_{x,i} E_{x,i}^2\right) \delta_{\sum_x n_x, Q} \\ &= \prod_x \sum_{\phi_x \in \mathbb{Z}(3)} \prod_x \frac{1}{3} \sum_{n_x} \phi_x^{n_x} \prod_{x,i} \sum_{E_{x,i}} \left(\phi_x^* \phi_{x+\hat{i}}\right)^{E_{x,i}} \exp\left(-g' \sum_{x,i} E_{x,i}^2\right) \delta_{\sum_x n_x, Q}. \end{aligned} \tag{4.6}$$

Now the sums over $E_{x,i}$ and n_x have decoupled and can therefore be calculated separately. The former can easily be summed explicitly,

$$\begin{aligned} \sum_{E_{x,i}} \left(\phi_x^* \phi_{x+\hat{i}}\right)^{E_{x,i}} \exp(-g' \sum_{x,i} E_{x,i}^2) &= 1 + \left(\phi_x^* \phi_{x+\hat{i}}\right)^{-1} \exp(-g') + \phi_x^* \phi_{x+\hat{i}} \exp(-g') \\ &= 1 + 2\,\mathrm{Re}\left(\phi_x^* \phi_{x+\hat{i}}\right) \exp(-g'). \end{aligned} \tag{4.7}$$

In the case without quarks, i.e. setting all $n_x = 0$, the partition function then simplifies to

$$Z_f = \prod_x \sum_{\phi_x \in \mathbb{Z}(3)} \prod_{x,i} \left[1 + 2\,\mathrm{Re}\left(\phi_x^* \phi_{x+\hat{i}}\right) \exp(-g')\right]. \tag{4.8}$$

The corresponding partition function of the Potts model takes the form

$$Z_p = \prod_x \sum_{\phi_x \in \mathbb{Z}(3)} \prod_{x,i} \exp(\kappa \delta_{\phi_x, \phi_{x+\hat{i}}}). \tag{4.9}$$

For the two models to be equivalent, the two partition functions have to be the same up to a constant factor, i.e.

$$Z_f = C^{dV} Z_p, \tag{4.10}$$

where C may depend on the coupling constants, d is the number of dimensions and V is the volume. Therefore dV is the number of bonds. The factor enters because as the next step we calculate C at a specific bond, where the above relation implies the two equations

$$\begin{aligned} 1 + 2\exp(-g') &= C\exp(\kappa), & \phi_x &= \phi_{x+\hat{i}}, \\ (1 - \exp(-g'))C &= 1, & \phi_x &\neq \phi_{x+\hat{i}}. \end{aligned} \tag{4.11}$$

The second relation defines the constant C and by dividing the equations we obtain a relation between κ and g',

$$\begin{aligned} C &= \frac{1}{1 - \exp(-g')}, \\ \exp(\kappa) &= \frac{1 + 2\exp(-g')}{1 - \exp(-g')}. \end{aligned} \tag{4.12}$$

Using these equations, it is now clear that the two models are equivalent in the case without quarks. When adding quarks we only need to notice that $\phi_x^{n_x}$ in the Potts model corresponds directly to $\phi_x^{n_x}$ in the flux model. Therefore the equivalence is also true in the case with quarks and the n_x play the same role as they did in the Potts model.

4.3. Worm algorithm

The flux model can be efficiently simulated using a so-called worm algorithm as originally proposed (for a different model) by N. Prokof'ev and B. Svistunov [13, 14]. The algorithm explained here is mainly based on [2].

The idea behind the worm algorithm in our case is to introduce an explicit violation of the constraint (4.1) by changing the value of a flux. This, in fact, violates the constraint in two points. At one of them, called the head, the constraint is then repaired, moving the worm head one step in some direction. This procedure is repeated until the head meets the tail at which point the constraint is again satisfied everywhere. If all these steps are performed with the correct probability this algorithm is ergodic in the flux variables (but not yet in the charges which will be solved later) and detailed balance is fulfilled as well (as explained in [2]). Another way of looking at this algorithm is saying that we use a standard Metropolis algorithm in an enlarged configuration space (where the constraint doesn't hold) using a few modifications (like not actually fully randomly choosing the next point and direction where a change should be proposed). This thinking naturally leads to the following concrete version of the algorithm:

1. **Start worm:** Randomly choose a site s, a direction $\hat{i}$ and a new flux value f. Accept this new configuration with probability $\exp(-\Delta S)$, where S is defined as in eq. (4.2) even though eq. (4.1) is not valid anymore. If it is not accepted then the sweep is over and nothing changes. Otherwise s is called the tail of the worm, $x := s + \hat{i}$ is called the head of the worm and we proceed with the next step.

2. **Try moving the worm:** Starting at x, choose randomly a new direction $\hat{i}$ and a new flux f. Then check whether this change repairs the constraint at point x. If so, accept it with probability $\exp(-\Delta S)$. If it is accepted, set $x = x + \hat{i}$. Otherwise (or if the constraint was not repaired at point x), change nothing. If the new x is equal to s, then the sweep is over. Otherwise repeat step 2.

After these steps, we have either added an arbitrary closed loop of fluxes or changed nothing. In both cases the constraint is again fulfilled at every point. However, as has been mentioned, we cannot stop here because we haven't moved the quarks at all yet. We therefore add other steps to the algorithm. We used two different quark moving steps:

1. **Move entire baryons:** Randomly choose two independent sites x and y. If n_x equals 3 and n_y is 0, move the baryon, i.e. the three charges, from x to y. We don't need to check for acceptance because this move doesn't change the action and is therefore always accepted.

2. **Move a single quark:** Choose one of the charges n_x at a random point x and a direction $\hat{i}$. If $n_{x+\hat{i}} < 3$, then propose moving a quark from x to $x + \hat{i}$. To fulfill the constraint this implies a new flux f for $E_{x,i}$ (or $E_{x+\hat{i},-i}$ depending on the sign of i). Therefore we accept this change with probability $\exp(-\Delta S)$ if $f \in \{-1, 0, 1\}$. Otherwise we change nothing.

Adding these two steps to the algorithm finally makes it ergodic. Detailed balance is fulfilled as well. An important other fact is, that the relative number of all these steps is important for the behavior of the autocorrelation. E.g. applying these quark moves twice in every sweep (while just creating one worm) instead of just once actually decreases the autocorrelation for small values of κ and thereby the statistical error (for large values of κ this changes nothing). This is partly due to the fact that moving quarks more often (i.e. more than just one step per quark) makes the difference between this and the previous configuration bigger. An example of this behavior is shown in figure 9. It shows binning curves which should converge to the uncorrelated statistical error $\sigma_{\mathcal{O}}$ of an observable $\mathcal{O}$ (see appendix A for more details), which in this example is the expectation value of the action, $\langle S \rangle$. As can be clearly seen, the curve on the left where the quarks are moved only one step per sweep converges to a value nearly twice as high as the one in the plot on the right side where the quarks were moved up to 10 times per sweep. Also, the number of steps which are needed to reach convergence is drastically smaller on the right. This number is a measure of the correlation time and the figures show therefore that this change also decreases the autocorrelation significantly.

Finding the optimal relative values seems to be a problem which can be solved in the easiest way by simply trying different numbers. Doing this led us to a rather dramatic decrease in the autocorrelation time and therefore in the overall error (for a fixed amount of computer time).

4.4. Calculating the observables

Using the algorithm above we can easily calculate the expectation value of observables as a function of g'. However, we are interested in the flux model only as a representation of the Potts model. Therefore we would prefer to calculate these as a function of κ instead.

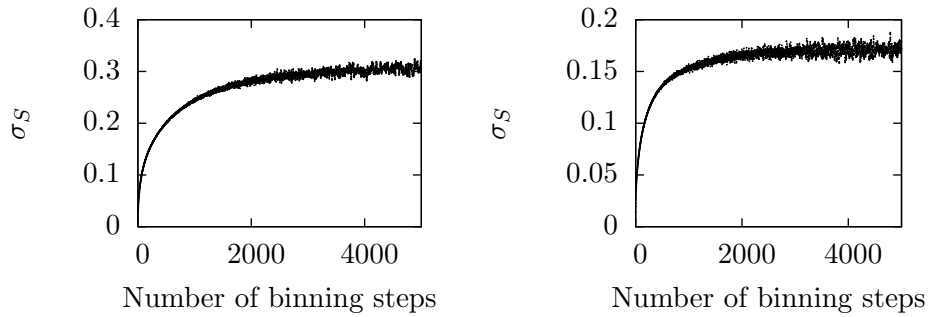

Figure 9: Correlation behavior of the worm algorithm for the flux model moving each quark once per sweep (left) or 10 times per sweep (right).

We start by explicitly calculating from eq. (4.12) what g' is in terms of κ, namely

$$g' = -\ln\left(\frac{\exp(\kappa)-1}{\exp(\kappa)+2}\right), \tag{4.13}$$

and therefore (as we will need it later on)

$$\frac{\partial g'}{\partial \kappa} = \frac{3\exp(\kappa)}{2-\exp(\kappa)-\exp(2\kappa)}. \tag{4.14}$$

As we have seen, the two partition functions are related by

$$Z_p = Z_f C^{dV}, \quad C = \frac{1}{1-\exp(-g')}. \tag{4.15}$$

Together these equations allow us to reformulate the expectation value of the action in terms of the flux model variables. We have already seen that

$$\langle S[\phi]\rangle_p = -\kappa\frac{\partial \log Z_p}{\partial \kappa} = -\kappa\frac{\partial \log(Z_f C^{dV})}{\partial \kappa} = -\kappa\left(\frac{\partial \log(Z_f)}{\partial \kappa} + dV\frac{\partial \log C}{\partial \kappa}\right), \tag{4.16}$$

where $\langle\cdot\rangle_p$ denotes an expectation value calculated with the partition function of the Potts model and where Z_p is the partition function of the Potts model. The factors can then explicitly be calculated, the first one yielding

$$-\kappa\frac{\partial \log(Z_f)}{\partial \kappa} = -\kappa\frac{1}{Z_f}\frac{\partial Z_f}{\partial g'}\frac{\partial g'}{\partial \kappa} = \left\langle \frac{\kappa}{g'}\frac{\partial g'}{\partial \kappa} S_f \right\rangle_f, \tag{4.17}$$

where S_f is the flux model action and $\langle\cdot\rangle_f$ denotes a flux model expectation value. The second factor simplifies to

$$dV\frac{\partial \log(C)}{\partial \kappa} = \frac{dV}{C}\frac{\partial g'}{\partial \kappa}\frac{\partial C}{\partial g'} = \frac{dV}{1-\exp(-g')}\frac{\partial g'}{\partial \kappa}. \tag{4.18}$$

Putting everything together, we obtain an explicit formula for the expectation value of the Potts action within the flux model,

$$\langle S[\phi]\rangle_p = \kappa\frac{\partial g'}{\partial \kappa}\left(\frac{\langle S[E]\rangle_f}{g'} + \frac{dV}{\exp(g')-1}\right). \tag{4.19}$$

Calculating the expectation value of the susceptibility is somewhat different. In the Potts model it is defined as

$$\chi = \left\langle \frac{1}{V^2} |\sum_x \phi_x|^2 \right\rangle_p = \frac{1}{V^2} \sum_{x,y} \langle \phi_x \phi_y^* \rangle_p = \frac{1}{V} \sum_x \langle \phi_x \phi_{x_0}^* \rangle_p, \tag{4.20}$$

where the missing factor V in the last equation comes from summing only over one point instead of x and y (which is possible because of the translation invariance of the model). Looking back at the proof of the equivalence of the two models, we see that also here the factor $\phi_x \phi_y^*$ corresponds to adding a quark at x and an anti quark at the fixed point y. This translates to adding a charge at these positions and is, in fact, the very thing we are already doing implicitly when starting a worm. In this model, however, the expectation value can be simplified even more. As the charges are a separate quantity and don't actually enter the action, χ can be calculated as

$$\chi = \frac{1}{V} \frac{\sum_x Z_{x_0 x}}{Z_0} = \frac{1}{V} \frac{Z_0 + Z_2}{Z_0}, \tag{4.21}$$

where Z_0 is the flux model partition function, $Z_{x_0 x}$ is the partition function of the enlarged space with the constraint broken at the points x_0 and x (which may coincide leading to an unbroken constraint) and Z_2 is the partition function with the constraint being violated at exactly two points. As the partition function is actually proportional to the probability of being in one of these sectors (constrain obeyed or violated at two points), the susceptibility is equivalent to

$$\chi = \frac{1}{V} \left(1 + \frac{p_2}{p_0} \right), \tag{4.22}$$

i.e. 1 plus the ratio between the time spent with the constraint violated at two points and the time spent in the sector with the constraint being obeyed. Here p_2 and p_0 are the respective probabilities. This means that we just have to count how many times we are in each of these sectors while letting the worm grow (and close again).

5. Results

Using the flux model we are now able to circumvent all problems mentioned in previous chapters and we have a rather efficient algorithm with which we can try to produce a phase diagram of the Potts model approximation to lattice Yang-Mills theory with static color charges. The first step is to actually regain the well known result for the Potts model without additional charges which will serve here as an explanation of the techniques we use for locating the position of the phase transition (if there is one).

5.1. Phase transition of the Potts model without static color charges

5.1.1. Possible transitions

Phase transitions are categorized according to their behavior in the continuum limit. Generally there are three different cases:

1. **First order phase transitions:** These are characterized by being discontinuous at the transition point. An example of this is shown in figure 10a.

2. **Second order phase transitions:** Here the order parameter itself remains a smooth function. However its derivative still is discontinuous at the transition point resulting e.g. in what is shown in figure 10b.

3. **Crossovers:** This is the weakest kind of transition possible. It is not actually a phase transition anymore but just a smooth crossover from one state to the other where everything remains continuous as shown in figure 10c.

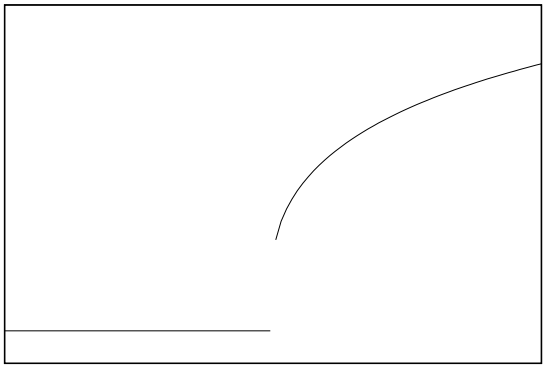

(a) Order parameter at a first order phase transition

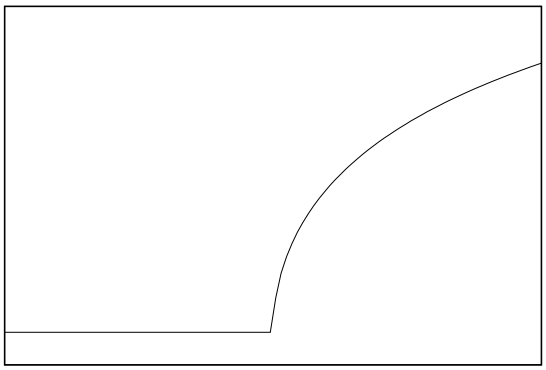

(b) Order parameter at a second order phase transition

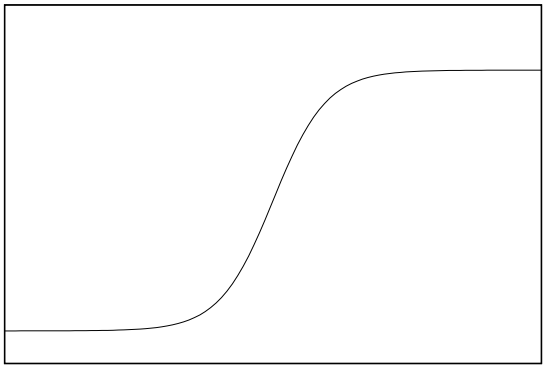

(c) Order parameter at a crossover

Figure 10: Possible transitions between two different phases.

5.1.2. Potts model phase transition

After verifying the correctness of the program with the methods explained in appendix B, we executed the simulation on a 3-dimensional lattice with 20 points per dimension, i.e. on a $V = 20^3$ lattice. As explained before, we use the expectation value of the action (per volume) of the Potts model and the susceptibility as observables. The results of these simulations are shown in figure 11. The statistical errors are too small to be visible. In the susceptibility plot it can clearly be seen that there is a phase where $\chi = 0$ which lasts up to $\kappa_T \approx 0.55$ and another phase with the susceptibility significantly bigger than zero with a rapid transition in between. Also the expectation value of the action shows a difference between these phases with a transition in between, although there this is somewhat less pronounced. Locating the exact point directly from this plot is actually very difficult. However, as mentioned before, it is well known that this transition is first order, in the continuum limit both observables are not continuous at the transition point. There is a jump which gets washed out on the lattice leading to curves as in figure 11.

Using this knowledge we can locate the point of the phase transition approximately (i.e. apart from corrections from finite-size scaling effects): It is at the point with the biggest (numerical) derivative. We approximate the derivative by finite differences, i.e. for an observable $A(\kappa)$ with a step size $\Delta\kappa$ between different measurements of $A(\kappa)$ we calculate

$$\frac{\partial A(\kappa_0 + \frac{\Delta\kappa}{2})}{\partial\kappa} \approx \frac{A(\kappa_0 + \Delta\kappa) - A(\kappa_0)}{\Delta\kappa}. \tag{5.1}$$

Note that the derivative is defined at $\kappa_0 + \frac{\Delta\kappa}{2}$, i.e. in between two measurements. To judge the accuracy of the point we located, we have to calculate the error of this estimation. Obviously we cannot get the transition point from this calculation with an accuracy better than $\Delta\kappa$. Moreover it is helpful to consider the error of the derivative itself because (as we will see) this transition gets weaker if we increase the number of charges and then we need to be able to judge whether two adjoining points are equal within errors. To calculate the error we can identify two sources: First there is the known error of $A(\kappa)$ itself which can easily be propagated to the derivative by using Gaussian error propagation applied to eq. 5.1. Second, we introduce an error with the discretization. This second error can be estimated by calculating the next order contribution to eq. 5.1 which is given by

$$\frac{\partial A(\kappa_0)}{\partial\kappa} = \frac{A(\kappa_0 + \Delta\kappa) - A(\kappa_0)}{\Delta\kappa} - \frac{1}{2}\frac{\partial^2 A(\kappa_0)}{\partial\kappa^2}\Delta\kappa + O(\Delta\kappa^2). \tag{5.2}$$

The term $\frac{\partial^2 A(\kappa_0)}{\partial\kappa^2}$ can be approximated by

$$\frac{\partial^2 A(\kappa_0)}{\partial\kappa^2} = \frac{A(\kappa_0 + \Delta\kappa) + A(\kappa_0 - \Delta\kappa) + 2A(\kappa_0)}{\Delta\kappa^2} + O(\Delta\kappa^2). \tag{5.3}$$

Therefore inserting this back into eq. 5.2 and taking the second term as an approximation to the error we finally get for the error of the derivative

$$\sigma_{\text{deriv}} \approx \sigma_{\text{gauss}} + \frac{1}{2}\frac{A(\kappa_0 + \Delta\kappa) + A(\kappa_0 - \Delta\kappa) + 2A(\kappa_0)}{\Delta\kappa}. \tag{5.4}$$

Calculating the derivative and this error for the measurement shown in figure 11 yields what is shown in figure 12. Both plots show a clear maximum at the same point. Looking directly at the data, we can locate the transition point at $\kappa_T = 0.55075 \pm 0.00025$ which is consistent with $\kappa_T \approx 0.55056$ from the literature [1].

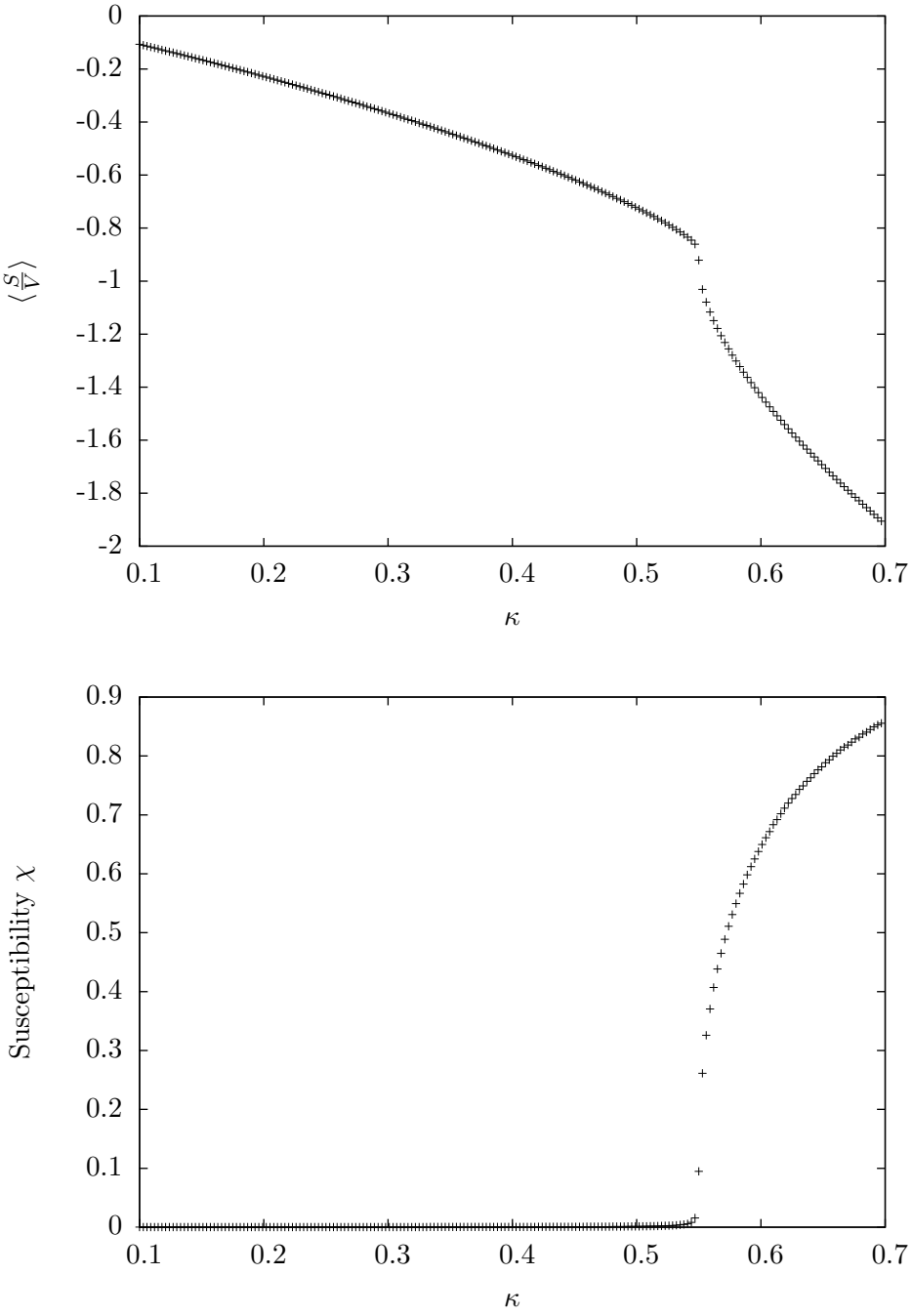

Figure 11: Plots of the considered observables as a function of the coupling κ on a $V = 20^3$ lattice without static color charges.

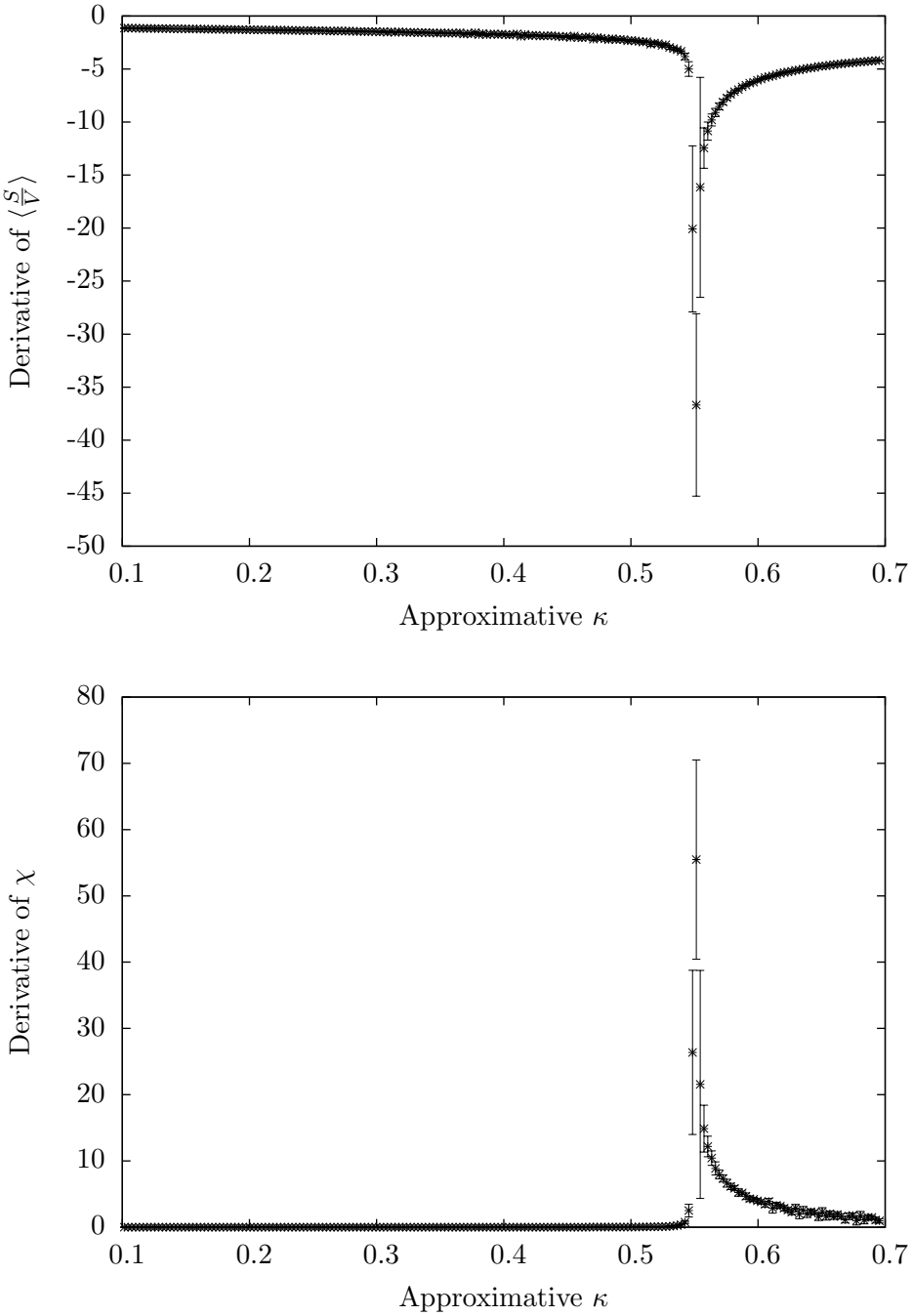

Figure 12: Plots of the derivatives of the observables considered as a function of the coupling κ on a $V = 20^3$ lattice without static color charges.

5.2. Adding color charges

After having confirmed the correctness of our algorithms, the last remaining step is to obtain the phase diagram of the model as a function of the number of color charges from simulations. The parameter we actually use for representing the number of quarks in a simulation is the baryon density n_B which we define as

$$n_B = \frac{Q}{3V}, \tag{5.5}$$

where Q is the number of color charges or "quarks" and V is the volume of the system. Obviously the baryon density has only a discrete set of allowed values because $Q \in \{0, 1, ..., 3V\}$. Using a further symmetry of the model explained in the next section we may notice that we actually need to simulate only one half of these values in order to be able to get a full phase diagram.

5.2.1. Baryon density symmetry of the Potts model

The Potts model with static color charges defined by the partition function of eq. (3.8) is invariant under the global transformation

$$n'_x = 3 - n_x, \tag{5.6}$$

i.e. under exchange of positions filled with color charges and positions without. This could be described as changing "holes" into color charges and vice versa. Calculating the transformed partition function yields again the partition function of eq. (3.8), because

$$\begin{aligned}
Z' &= \prod_x \sum_{\phi_x \in \mathbb{Z}(3)} \sum_{n'_x=0}^{3} \exp(-S[\phi]) \delta_{\sum_x n'_x, Q'} \prod_x \phi_x^{n'_x} \\
&= \prod_x \sum_{\phi_x \in \mathbb{Z}(3)} \sum_{n_x=0}^{3} \exp(-S[\phi]) \delta_{\sum_x (3-n_x), Q'} \prod_x \phi_x^{3-n_x} \\
&= \prod_x \sum_{\phi_x \in \mathbb{Z}(3)} \sum_{n_x=0}^{3} \exp(-S[\phi]) \delta_{\sum_x n_x, 3V-Q'} \prod_x \phi_x^{-n_x} \\
&= \prod_x \sum_{\phi_x \in \mathbb{Z}(3)} \sum_{n_x=0}^{3} \exp(-S[\phi]) \delta_{\sum_x n_x, 3V-Q'} \prod_x \phi_x^{n_x} = Z,
\end{aligned} \tag{5.7}$$

where we used that $\phi^3 = 1 \, \forall \phi \in \mathbb{Z}(3)$ and the fact that it doesn't matter whether we sum over all values of ϕ_x or of ϕ_x^{-1}. Here Q' is the number of color charges after the transformation. Therefore $Q = 3V - Q'$ is the number of color charges we had before applying the transformation. For our simulations this implies that we actually need to look only at baryon densities $n_B \leq 0.5$ as above this we will get nothing but a mirror image of the same results.

5.3. The phase diagram

We have used the above procedure to evaluate different baryon densities. This resulted in the plot shown in figure 13. The bars above and below each point correspond to the width of the peak in diagrams like in figure 12. We see that the transition gets broader as we increase the baryon density. Moreover it seems to be moving to smaller values of κ_T with increasing n_B, although this is not conclusively decidable from this plot.

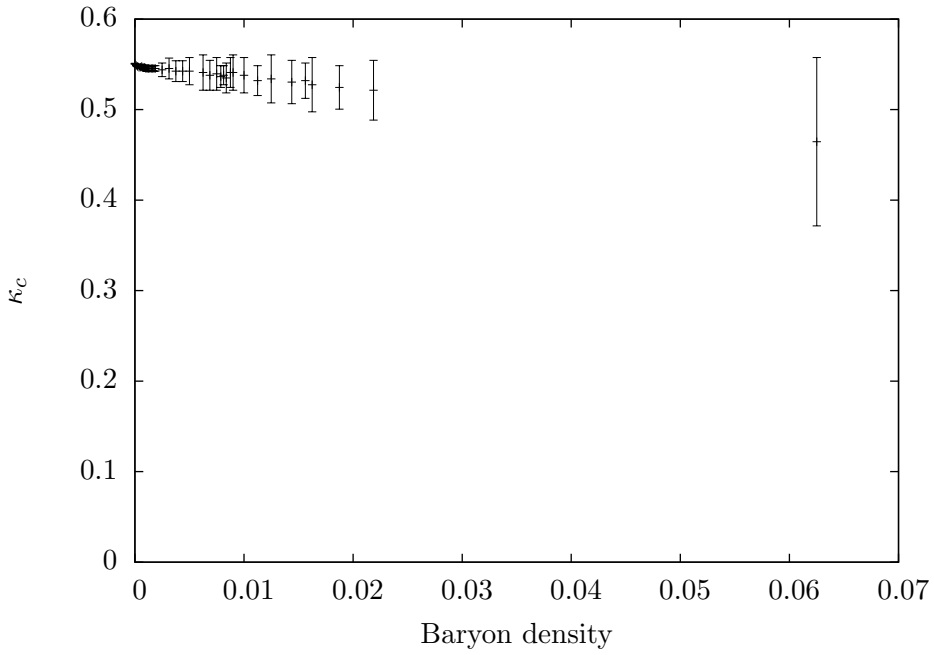

Figure 13: Phase diagram of the Potts model. The error bars are a measure of the derivative's peak width.

5.3.1. Small baryon densities

We now look at a part of figure 13 in more detail which is shown in figure 14. We see that for the first few values the transition point is lowered but the width stays the same. The width in this part is primarily determined by our step size, i.e. by the smallest difference between values of the coupling κ we evaluated. However looking only at this plot hides a significant detail: If we look at the actual results of these runs, i.e. at the susceptibility itself, and plot it for different volumes we get what is shown in figures 15 and 16. The first one, at vanishing baryon density, shows a clear change with increasing volume. There seems no doubt that this will become an actual jump in the infinite volume limit. Figure 16 shows only the biggest and the smallest volume considered in figure 15 for a slightly increased baryon density $n_B = 0.000375$, i.e. with only 3 additional baryons. Even though this seems like a small change of the density, we already see a very different picture. It doesn't seem clear at all what happens to this in the infinite volume limit. It may still be a (very weak) first order transition or it may have turned into a second order transition. Deciding this is not possible from these plots, we would need to perform a finite size scaling analysis which is outside the scope of this thesis. We can also plot the behavior of the susceptibility for different baryon densities in a fixed volume. This is shown in figure 17. Note that the difference between consecutive baryon densities is exactly one baryon, i.e. the smallest change allowed. We see here also that the transition becomes slower with increasing baryon density. This implies again that the first order transition gets weaker, most probably turning into a second order transition at some point. However, we cannot extract this point from our data, a more extensive search would be needed to be able to conclusively decide on the order of the transition at every point of the diagram.

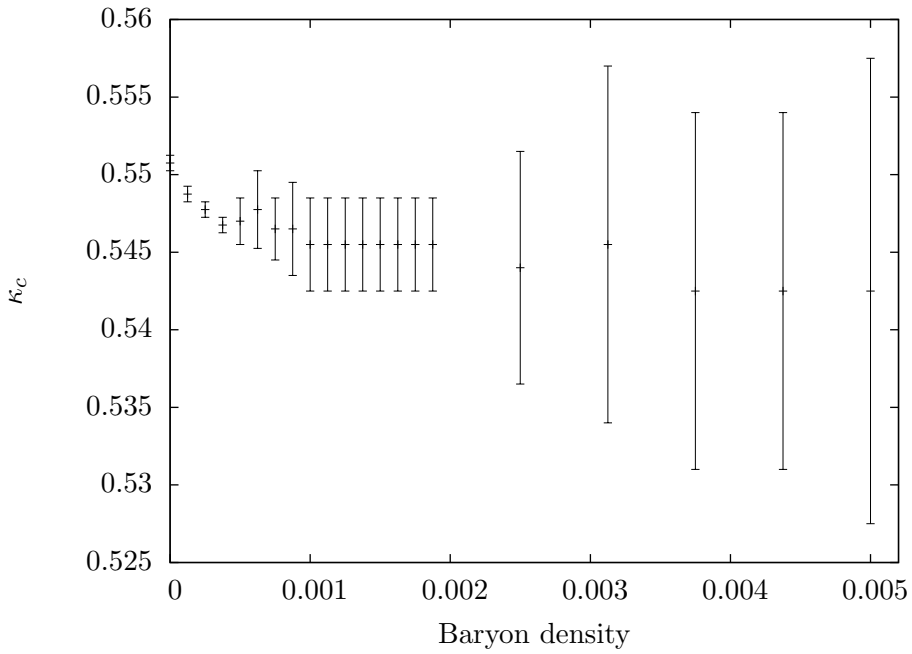

Figure 14: Enlargement of a part of the phase diagram.

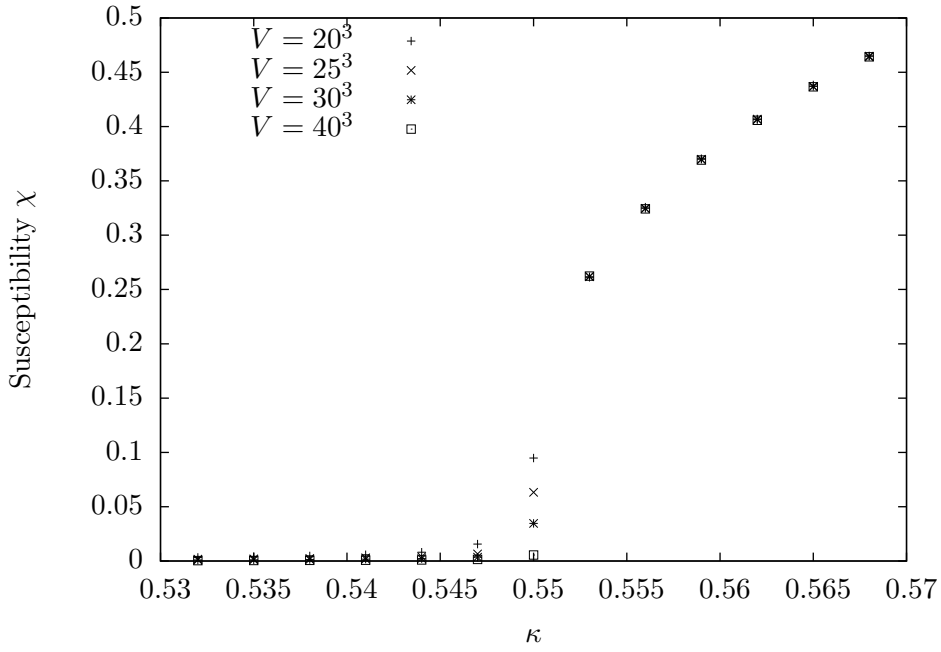

Figure 15: Volume dependence of χ at $n_B = 0$.

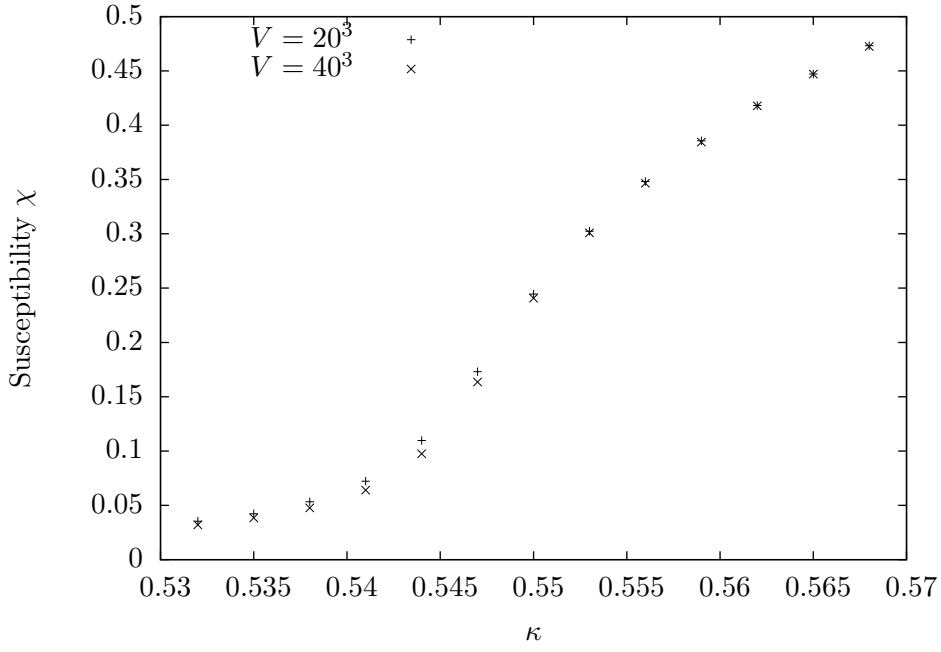

Figure 16: Volume dependence of χ at $n_B = 0.000375$.

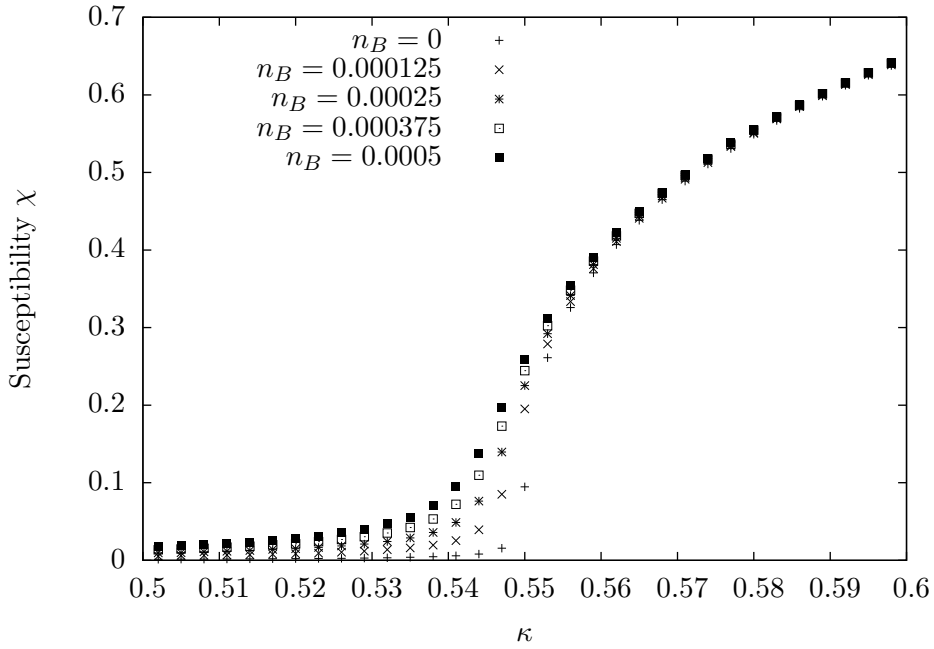

Figure 17: Baryon density dependence of χ.

5.3.2. Large baryon densities

After having investigated very small baryon densities, let us now look at large values of it. Figure 18 shows what happens for the largest possible baryon density $n_B = 0.5$. Note that the fluctuations of points for small κ is of no physical origin. It is an artifact of an inefficiency of the worm algorithm leading to a much larger statistical error of these points than what we get for other values of κ (this is actually the reason why the error-bars are omitted in this plot). This interpretation is also supported by the fact that the expectation value of the Potts model action shows no such behavior at all as can be clearly seen in figure 19. Unfortunately we didn't have time to further investigate this problem and try to solve it. Figure 18 still shows that there clearly remains no first or second order phase transition. It seems to be gone, χ is significantly bigger than 0 for every value of κ. This means that the system is always in the deconfined phase independent of the temperature.

Figure 20 shows the susceptibility of the largest baryon density still included in figure 13, $n_B = 0.0625$. Apart from the same problem with small values of κ it shows again no distinctive sign of a phase transition even though here it is not clear whether or not the system is in the confined phase for very small κ i.e. whether an actual transition remains. However, because the transition is, in fact, associated with the breaking of an exact symmetry of the Potts model and therefore there is a qualitative difference between the two states, it is not possible to have a crossover here. From our results though, we cannot tell what happens to the phase transition. Most likely it should just move to $\kappa_T = 0$ and thereby vanish afterwards. This could explain what we see in our results even though no indication of this move of the transition point is visible in figure 13 up to $n_B = 0.0625$. However, this question may be answered by simply collecting more data.

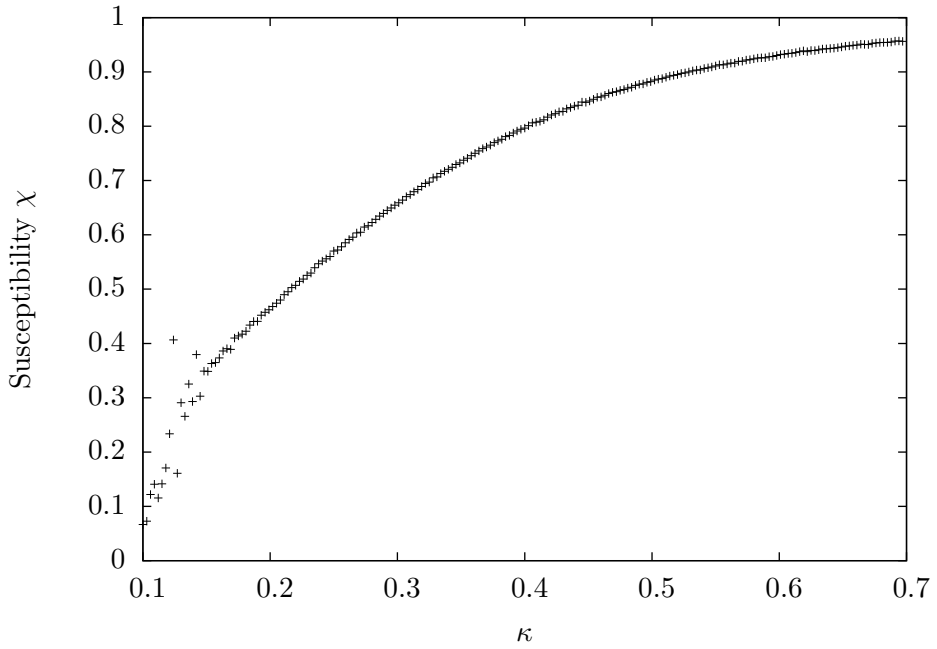

Figure 18: Susceptibility at $n_B = 0.5$.

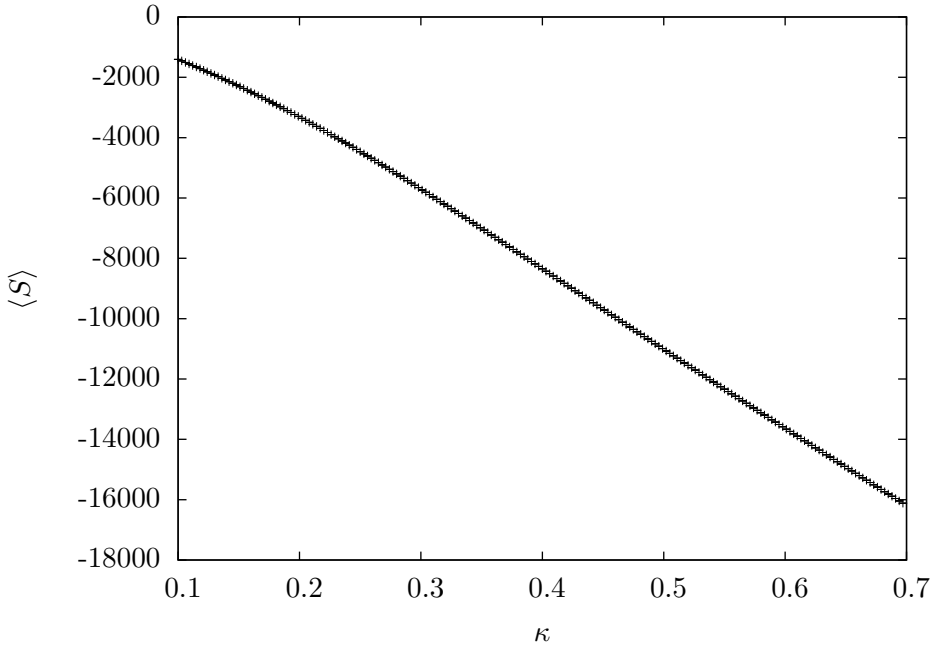

Figure 19: Expectation value of the action at $n_B = 0.5$.

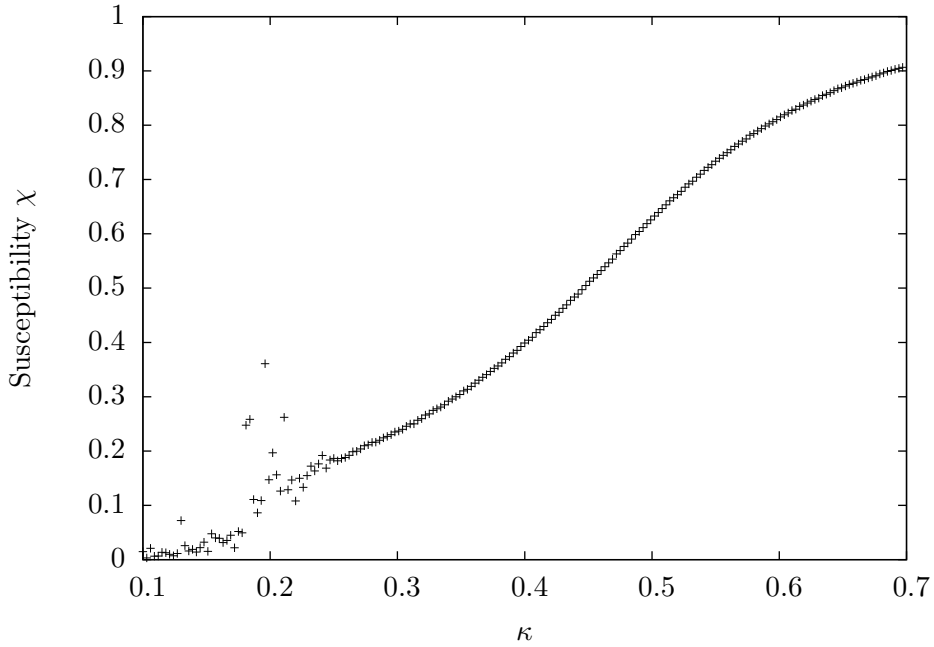

Figure 20: Susceptibility at $n_B = 0.0625$.

5.3.3. The susceptibility as a function of the baryon density

Instead of looking for a phase transition in plots at a fixed baryon density n_B, we can also consider plots at a fixed value of κ as a function of n_B. We have done this in figure 21. Apart from the same problem with the statistical errors getting big for small values of κ, we see that here we first have some densities for which (approximately) $\chi = 0$, then the value grows and soon gets significantly different from 0. This may be an indication that there is a transition for some n_{Bc}, i.e. that indeed the transition line in figure 13 moves down to $\kappa_T = 0$ with increasing baryon density. However we don't have enough data (and some of the errors are too big) to really be sure that this is what happens here.

Generating the same plot for different values of κ yields figure 22. We see that for the largest value of $\kappa = 0.697$ there is clearly no phase transition at all. The system is always in the deconfined phase. As expected, decreasing κ leads to smaller values of the susceptibility for small values of n_B until we reach $\kappa = 0.19$ where we cannot be sure whether we have a transition or not. It would be interesting to go to even smaller values of κ. In principle we would even have the data to do this. However, the errors then get so big that these plots become impossible to interpret.

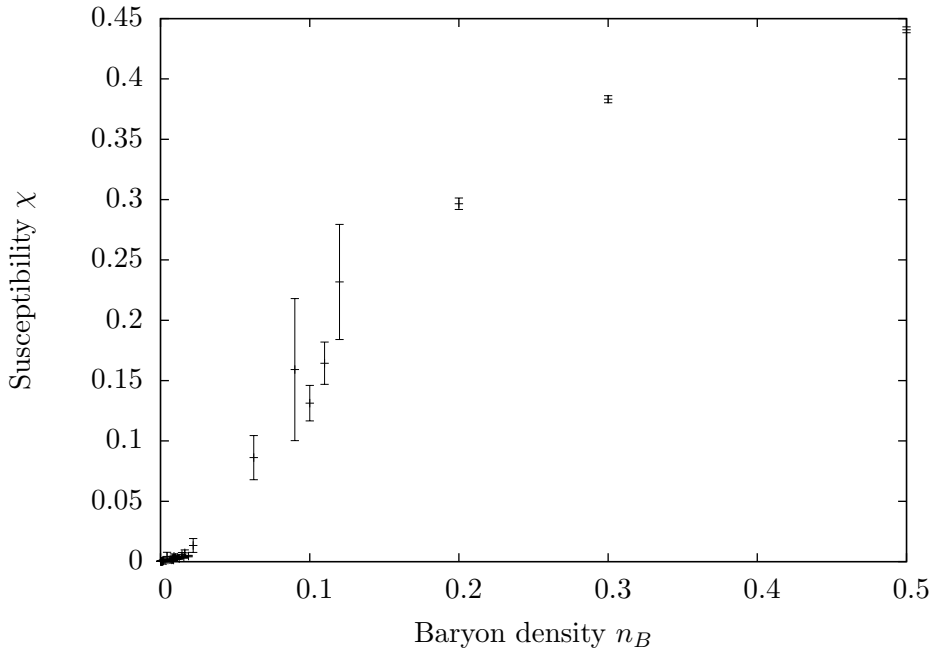

Figure 21: Susceptibility at $\kappa = 0.19$.

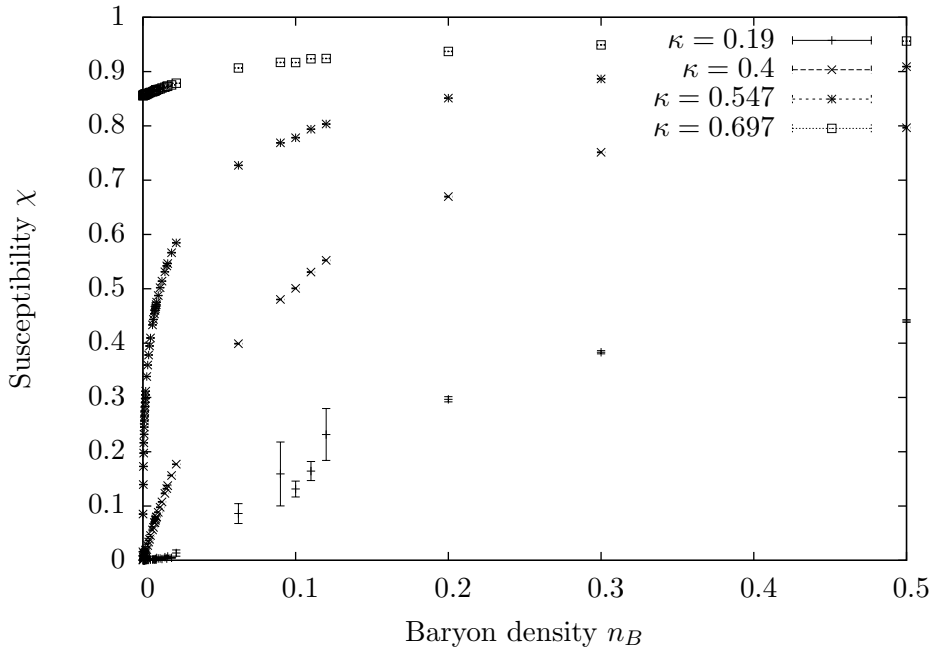

Figure 22: Susceptibility at different values of κ.

6. Conclusion and outlook

We investigated the phase diagram of the Potts model with a fixed number of static color charges avoiding the sign problem by switching to an equivalent flux representation. We found the already well-established first order phase transition for vanishing baryon density and saw that increasing the number of color charges weakens the transition more and more until it most likely turns into a second order transition. However, because of time constraints, we couldn't investigate this in more detail to find out the exact fate of the transition for higher baryon densities, though we have strong evidence that at some point the transition disappears completely.

The next step would obviously be to study at which point the transition turns from first to second order, e.g. by investigating the behavior on larger lattices. We think that this happens at small baryon densities where the inefficiency problem of the algorithm for small values of the coupling constant doesn't come into play yet. To see what happens further in the diagram, and especially to decide whether the second order transition terminates somewhere (which from theoretical arguments is impossible) or goes all the way down to $\kappa_T = 0$, we have to improve the algorithm. That is because its inefficiency for small couplings makes it impossible to extract meaningful results if the transition moves to values of the coupling smaller than $\kappa_T \approx 0.4$. This could possibly be achieved by making only a small change to our worm algorithm: It might suffice to add the possibility to move color charges in the worm itself instead of doing this as a separate step (as used for a somewhat different model in a recent paper [10]). Another idea is to add a step which can move the color charges by more than one lattice spacing at once. Though whether these ideas actually work needs to be tested in future work.

As a final conclusion, we can say that we have obtained part of the phase diagram of the Potts model with static color charges and we showed that it is possible to avoid sign problems by switching to a flux representation of the partition function which can be simulated quite efficiently using a worm algorithm.

A. Monte Carlo simulations and error analysis

A Monte Carlo simulation is a simulation which builds a Markov chain of configurations that models a given probability distribution approximatively. This means that the number of times a configuration appears is proportional to its probability, e.g. to its Boltzmann weight in statistical mechanics. Every configuration follows from its predecessor through a well-defined probabilistic manipulation. In order for this to be correct, two criteria have to be fulfilled. First the algorithm needs to be ergodic, i.e. every configuration must in principle be reachable with a non-zero probability. Second, it needs to fulfill detailed balance. This means that the probability to get from one configuration to another must be balanced to its inverse. What exactly is meant by this will be defined below. Both criteria together ensure that after waiting long enough the initial configuration doesn't matter anymore and that one gets a correct approximation to the given probability density.

The standard approach to fulfill these requirements in statistical mechanics is the so-called Metropolis algorithm. There every configuration $[\phi]$ has an associated action $S[\phi]$ and a Boltzmann weight $\exp(-S[\phi])$. One then proposes in every step (also called sweep) a new configuration $[\phi']$. The latter is then accepted with probability

$$\omega([\phi] \to [\phi']) = \min\{1, \exp(-S[\phi'] + S[\phi])\} \tag{A.1}$$

ensuring detailed balance, i.e. it fulfills [12]

$$P[\phi]\omega([\phi] \to [\phi']) = P[\phi']\omega([\phi'] \to [\phi]), \tag{A.2}$$

where

$$P[\phi] = \frac{\exp(-S[\phi])}{Z} \tag{A.3}$$

is the probability of the configuration $[\phi]$. Doing this a large number of times then allows us to generate an accurate distribution of configurations according to their Boltzmann weight (after omitting the first few configurations which still depend on the initial state).

A.1. Binning

Due to the fact that Monte Carlo simulations build a Markov chain, consecutive configurations naturally depend on each other. This implies that naively calculating the error of an observable $\mathcal{O}$, i.e. calculating its standard deviation

$$\sigma_{\mathcal{O}} = \sqrt{\frac{\langle \mathcal{O}^2 \rangle - (\langle \mathcal{O} \rangle)^2}{N-1}} = \sqrt{\frac{1}{N(N-1)} \sum_{i=1}^{N} (\mathcal{O}[\phi^{(i)}] - \langle \mathcal{O} \rangle)^2}, \tag{A.4}$$

doesn't yield the correct result, this expression actually underestimates it. To solve this, one uses a so-called binning procedure. Instead of calculating $\sigma_{\mathcal{O}}$ using every measurement $\mathcal{O}_i$ one uses averages of j subsequent measurements

$$\langle \mathcal{O} \rangle_{ij} = \frac{1}{j} \sum_{k=0}^{j-1} \mathcal{O}[\phi^{(i+k)}]. \tag{A.5}$$

j here is usually called the binsize. With this we generate a sequence of standard deviations

$$\sigma_{\mathcal{O}j} = \sqrt{\frac{1}{M(M-1)} \sum_{i=1}^{M} (\langle \mathcal{O} \rangle_{ij} - \langle \mathcal{O} \rangle)^2} \tag{A.6}$$

where $M = \frac{N}{j}$ is the number of bins. This quantity then converges to the uncorrelated statistical standard deviation of the measurements $\mathcal{O}_i$ as e.g. shown in figure 23. It clearly shows that the standard deviation converges to a certain value with increasing number of binning steps, i.e. with increasing binsize. Note that the fact that the curve gets broader at the end is due to M getting smaller and smaller with increasing binsize. Therefore the number of individual measurements contributing to the standard deviation $\sigma_{\mathcal{O}j}$ gets smaller as well, thereby increasing the error of the calculated value due to less statistics.

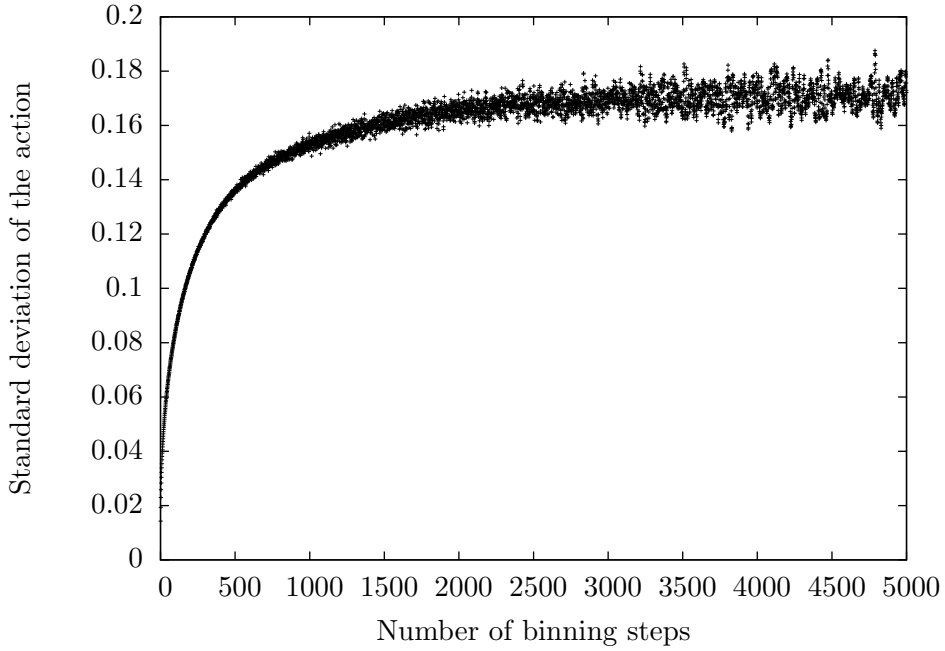

Figure 23: Example of a binning curve.

B. Verifying the implementation of the algorithms

To ensure the correctness of our programs we use the following different techniques:

- **Calculation by hand:** For very small lattices in one dimension the Potts model only has a very small number of possible configurations allowing us to calculate the partition function fully analytically.
- **Exact evaluation by a program:** For slightly larger lattices (up to $V \approx 2^3$) it is possible to calculate all configurations using a computer program.
- **Comparing the different algorithms:** Although most of the different algorithms presented in chapters 3 and 4 only work correctly in a subset of the whole configuration space (e.g. only for vanishing baryon density) there are still areas where some of them give correct results concurrently.

With these we can begin with the calculations by hand to ensure correctness of the exact programs. The latter then allow us to verify all algorithms on small lattices. The independent algorithms finally were used to ensure that all of them give the same result in their respective subspaces of the configuration space where they work correctly.

Acknowledgements

I would like to thank Uwe-Jens Wiese for his support during the last year when we were working on this thesis together. He always helped me and explained everything I needed to know in as much detail as necessary. Working with him was very pleasant. I would also like to thank my bureau colleague Kyle Steinhauer for patiently listening to all the problems I encountered. He helped me wherever possible even though he wasn't directly involved in my work and had enough to do working on his own problems. Finally I'd like to thank all my friends and my family for their support during this time.

References

[1] M. Alford, S. Chandrasekharan, J. Cox, and U.-J. Wiese. Solution of the complex action problem in the Potts model for dense QCD. *Nucl. Phys. B*, 602:61–86, 2001.

[2] M. Bögli. Worm algorithm in the O(N) model and related models. Master thesis, Universität Bern, 2010.

[3] S. Chandrasekharan and U.-J. Wiese. Meron-Cluster Solution of Fermion Sign Problems. *Phys. Rev. Lett.*, 83:3116–3119, 1999.

[4] J. Condella and C. DeTar. Potts flux tube model at nonzero chemical potential. *Phys. Rev. D*, 61, 2000.

[5] T. DeGrand and C. DeTar. Phase structure of QCD at high temperature with massive quark density: A Z(3) paradigm. *Nucl. Phys.*, 225:590–620, 1983.

[6] Z. Fodor and S. D. Katz. The phase diagram of quantum chromodynamics. *arXiv: 0908.3341v1*, 2009.

[7] P. Henelius and W. Sandvik. The sign problem in Monte Carlo simulations of frustrated quantum spin systems. *Phys.Rev. B*, 62:1102, 2000.

[8] K. Holland and U.-J. Wiese. The center symmetry and its spontaneous breakdown at high temperatures. In M. Shifman, editor, *At the frontier of particle physics: A handbook of QCD*, pages 1909–1944. World Scientific, 2001.

[9] L. McLerran and B. Svetitsky. Quark liberation at high temperature: A Monte Carlo study of SU(2) gauge theory. *Phys. Rev. D*, 24:450, 1981.

[10] Y. D. Mercado, H. G. Evertz, and C. Gattringer. The QCD phase diagram according to the center group. *arXiv: 1102.3096v1*, 2011.

[11] I. Montvay and G. Münster. *Quantum Fields on a Lattice*. Cambridge University Press, 1994.

[12] F. Niedermayer. *Notes on Monte Carlo Simulations of Systems in Thermal Equilibrium*. Universität Bern, 2006.

[13] N. Prokof'ev and B. Svistunov. Worm algorithms for classical statistical models. *Phys. Lett. A*, 81(16):160601, 2001.

[14] N. Prokof'ev, B. Svistunov, and I. Tupitsyn. "Worm" algorithm in quantum Monte Carlo simulations. *Phys. Lett. A*, 238(4-5):253–257, 1998.